1981ApJ...249..270V

THE ASTROPHYSICAL JOURNAL, 249:270–289, 1981 October 1
© 1981. The American Astronomical Society. All rights reserved. Printed in U.S.A.

STELLAR CORE COLLAPSE. I. INFALL EPOCH[1]

KENNETH A. VAN RIPER
Department of Physics, University of Illinois at Urbana-Champaign
AND
JAMES M. LATTIMER
Department of Earth and Space Sciences, State University of New York at Stony Brook
Received 1981 January 15; accepted 1981 April 3

ABSTRACT

We report on simulations of the collapse of the central iron core of a 15 $M_\odot$ spherically symmetric star. In this paper we consider the infall epoch, between the onset of collapse and core bounce. The models use the recent equation of state of Lamb, Lattimer, Pethick, and Ravenhall and general-relativistic hydrodynamics. The electron capture rates on nuclei proceed rapidly for densities less than 10^{11} g cm^{-3}, but are suppressed at higher densities where the neutron number of the nucleus, N, exceeds 40 (Fuller, Fowler, and Newman). We treat neutrino transport by a leakage scheme. The effects of changes in the neutrino trapping density and of qualitative changes in the electron capture reactions on the evolution are explored. Greater lepton loss during collapse leads to larger pressure deficits, more rapid collapse, and smaller inner homologous cores. The entropy change during the infall is small—$|\Delta s| < 0.8$. The mass of inner core is given, to about 20%, by the formula of Goldreich and Weber. Because the collapsing core is far from equilibrium, the effects of general relativity are small.

Subject headings: dense matter — equation of state — hydrodynamics — stars: collapsed — stars: interiors

I. INTRODUCTION

Evolutionary calculations of nonrotating stars with masses in the approximate range $10\ M_\odot \lesssim M \lesssim 70\ M_\odot$ all show the development of an unstable core, containing about 1.5 $M_\odot$ of iron, which undergoes dynamic collapse (Arnett 1977*a*; Barkat 1977; Weaver, Zimmerman, and Woosley 1978). It is thought that this event is somehow associated, perhaps even causally, with Type II supernova explosions. The disruption of these massive stars, resulting from an explosion within the core, can account for the abundance of elements between oxygen and the iron peak elements (Arnett 1978; Weaver and Woosley 1980), as well as the *r*-process elements. The abundances within the supernova remnants Cas A (Chevalier and Kirshner 1978) and Pup A (Canizares and Winkler 1981) suggest that they contain material from the stellar mantle. The structure of the Cas A remnant can be explained by invoking mass loss from a giant star prior to the explosion (Lamb 1978). If extensive mass loss does not take place prior to the explosion, the outer layers of these massive stars form a red giant structure. An impulsive energy release of about 10^{50} ergs within such an extended envelope accounts for observed Type II supernova light curves (Grasberg, Imshennik, and Nadyozhin 1971; Lasher 1975; Chevalier 1976; Arnett and Falk 1976). The large gravitational energy release ($\sim 10^{53}$ ergs) in the collapse of the stellar core to a neutron star is more than enough to power the supernova (Baade and Zwicky 1934) and disrupt the star.

Several theoretical models have been reported in which an explosion follows core collapse (Colgate and White 1966; Arnett 1967; Schwartz 1967; Wilson 1971, 1980*a*; Bruenn 1975). With improved input physics, however, no current numerical collapse simulations show an explosion. It is agreed that the core, if it is nonrotating, collapses until it reaches nuclear density. At that point the core has divided into an inner homologous (velocity proportional to the radius) core and an outer core, which is collapsing supersonically. If a black hole is not formed directly, the inner core bounces somewhere above nuclear density. A shock wave forms between the rebounding or stationary inner core and the infalling outer core.

This shock plays a key role in most proposed explosion mechanisms. Whether or not an explosion occurs, and how energetic it is, depends on the strength of the shock wave. (The velocity of the shock front, the entropy and velocity jumps across the shock, etc., all increase with, and serve as a measure of, the shock strength.) It has been proposed, although on the basis of adiabatic models, that the simple hydrodynamic formation and propagation of the shock can, depending on the equation of state, directly result in an explosion (Van Riper 1978; Lichtenstadt, Sack, and Bludman 1980). In this case the explosion energy increases with the shock strength. Deposition

[1] Research supported in part by NSF grant PHY78-04404 at the University of Illinois and USDOE grant DE-AC02-80ER10719 at the State University of New York.

© American Astronomical Society • Provided by the NASA Astrophysics Data System

1981ApJ...249..270V

mechanisms, where the neutrinos emanating from the hot matter behind the shock deposit either energy (Colgate and White 1966) or momentum (Schramm and Arnett 1975) in the overlying matter, thus resulting in the expansion of that matter, have also been suggested. The deposition mechanisms are sensitive to the neutrino energy (neutrino-matter cross sections are proportional to the square of the neutrino energy). Since neutrinos originating behind the shock have thermal energies (Bethe, Applegate, and Brown 1980), a strong shock, where postshock temperatures are high, leads to more efficient deposition. Following bounce, a lepton inversion develops in the core. It was pointed out by Epstein (1979) that the core is then unstable to convection. Colgate (1978) and Colgate and Petschek (1980) have further suggested that this instability could lead to a dynamic overturn of the entire inner core, which would release a large number of high-energy neutrinos on the short dynamic time scale of the inner core. Explosion follows deposition of these neutrinos in the outer core. A positive entropy gradient, however, tends to stabilize the core and, if large enough, can inhibit overturn (Lattimer and Mazurek 1981). The entropy in the unshocked inner core is lower than in the overlying shocked matter. Overturn requires low postshock entropies, and hence a weak shock.

In any event the strength of the shock—or, equivalently, the entropy jump across the shock—is important in deciding the outcome of stellar collapse. The shock strength is determined primarily by the mass of the inner core, M_{IC} (Van Riper 1980). The gravitational acceleration of the outer core and the velocity of infall increase with the mass of the inner core. The velocity jump across the shock, which determines the entropy increase, is greater for faster preshock infall velocities, so that the stronger shocks result from larger inner core masses.

The inner core mass is decided during the infall epoch before bounce, and depends primarily on the pressure deficit (the ratio of the actual pressure to that required for equilibrium). Smaller pressures result in smaller masses. During infall the entropy is low enough for most of the nucleons to exist in nuclei. The pressure is then dominated by electrons (and also by neutrinos at high density). The pressure deficit, therefore, is determined by the number of leptons lost, in the form of escaping neutrinos, during infall.

The magnitude of the lepton loss depends on (1) the rate of electron capture $e + p \rightarrow n + \nu_e$, where the nucleons may be either inside or outside nuclei, (2) whether or not neutrinos, once created by the capture reactions, can escape from the star, and (3) the rate of collapse, which determines the time during which captures can proceed. In this paper we concentrate on how changes in the electron capture rates and the neutrino trapping density affect the final lepton fraction and inner core mass at bounce. Our models show the effect of suppressing the electron capture rate on heavy nuclei when the neutron number of the nucleus $N \geq 40$ (Fuller, Fowler, and Newman 1981). For these large neutron numbers the nucleus no longer has the shell structure of iron, on which our heavy capture rates are based (Bethe *et al.* 1979). The rate of collapse is determined in our hydrodynamic models by the pressure deficit and the equation of state.

There are a number of papers in the literature describing one-zone collapse models (see, for example, Sato 1975; Epstein, Nørgaard, and Bond 1979; Epstein and Pethick 1981). These models compute the change in lepton fraction and entropy during the collapse of a homogeneous sphere, but usually *assume* some collapse rate. Our more detailed models find that the collapse rate is much smaller than commonly used in these models, although we agree that the final lepton fraction and entropy are rather insensitive to the collapse rate. The one-zone models cannot, of course, compute the mass of the homologous inner core.

Our collapse models use a recent equation of state of hot, dense matter which self-consistently accounts for nuclear interactions among nucleons inside and outside nuclei (Lamb *et al.* 1978, 1981).

The equation of state, electron capture rates, neutrino transport scheme, and hydrodynamic method are described in the next section. The features of the initial model, which is the center of the 15 $M_\odot$ stellar evolutionary model of Weaver, Zimmerman, and Woosley (1978), just after the onset of dynamical collapse, are discussed in § III. Section IV is devoted to our results, including the effects of variations of the neutrino trapping density and the electron capture rates on the changes in lepton fraction and entropy during collapse and on the effective adiabatic index. We also discuss there the validity of homology assumptions. The importance of general relativity is considered in § V. We summarize our main findings in § VI.

II. MODEL

a) *Equation of State*

We use the equation of state of Lamb, *et al.* (1978, 1981; hereafter LLPR) between nuclear density and $\rho = 10^8$ g cm^{-3}. The baryon component in this equation of state consists of a typical heavy nucleus, α-particles, and neutrons and protons outside the nuclei. The interactions among the outside nucleons and among the nucleons in the nucleus are calculated using a temperature-independent phenomenological Skyrme interaction. Thermal effects (excitation spectra) of the nucleon gases (inside and outside the nucleus) are implicitly included through the interacting Fermi gas distribution of the nucleons (Lattimer and Ravenhall 1978). The energy of the heavy nucleus is described by the usual bulk, surface, Coulomb (including lattice effects), and translational terms. Minimization of the total free energy at a given temperature, baryon density, and electron fraction, subject to the constraints of mass and charge conservation, determines the abundance of the various species, the mass number A, and the proton number Z, of the average nucleus. The electron-positron contributions to the equation of state were found by assuming the electrons to be relativistic Fermi gases and using the exact formulae of

© American Astronomical Society • Provided by the NASA Astrophysics Data System

1981ApJ...249..270V

Bludman and Van Riper (1978). Electron type neutrinos (ν_e, but not $\bar{\nu}_e$) were assumed to always have a Fermi distribution, and their thermodynamic contributions were those of a perfect Fermi gas. We included the neutrino chemical potential, μ_ν, in the electron capture energetics only when $\mu_\nu > 0$.

The equation of state was used in tabular form, with five entries per decade in density, ρ, 20 per decade in temperature T, and with steps of 0.05 in the electron fraction Y_e. In addition to the total pressure and internal energy density, we tabulated the neutron-proton chemical potential difference, the mass fraction of protons contained in the heavy nucleus, the mass fraction of outside protons, and the partial mean free path, $\lambda\epsilon_\nu{}^2\rho$. The latter four quantities are required for evaluating electron capture rates and the rate of neutrino escape. For any point in (T, ρ, Y_e)-space these quantities were evaluated by interpolation (logarithmic where suitable) between the neighboring eight table points. The table spacing was sufficiently fine for all quantities to vary smoothly with the independent parameters, except (1) at phase boundaries (e.g., the heavy nucleus–alpha transition) where inside and outside proton abundances and the partial mean free path reflect the rapidly changing composition, and (2) just below nuclear density where the strong interactions are important and the baryon pressure and energy change rapidly with density. The coarse spacing over the phase boundaries is not important along the infall trajectories, which remain in the heavy nuclei dominated region. In several of the figures accompanying this paper we have smoothed out "wiggles" due to the tabular form of the equation of state. Curves of entropy versus density, for example, show oscillations with amplitude $\Delta s = 0.02$ and a period exactly equal to the table spacing. Such noise has no significant effect on the evolution.

We used the LLPR equation of state only for densities in excess of 10^8 g cm^{-3}. At lower densities we treated the matter as an ideal gas with $\Gamma = \frac{4}{3}$. At lower densities in the precollapse star, nuclear burning, which we do not include in the model, is occurring. In addition the temperatures are too low to assume, as does the LLPR equation of state, that nuclear equilibrium obtains. The ideal gas assumption is thus no less valid than the LLPR equation of state for $\rho < 10^8$ g cm^{-3}. This low density matter is in the outer core, so it does not affect the evolution of the matter which will make up the inner core, and it does not encounter the shock wave until the fate of the shock has been decided at the higher densities of the neutrino photosphere.

b) *Electron Capture Rates*

i) *Capture on Heavy Nuclei*

The rate for electron capture on our average heavy nucleus is based on the Fermi gas approximation to the shell model description of electron captures introduced by Bethe *et al.* (1979; hereafter BBAL). They realized that, if the heavy nucleus has the shell structure of an iron peak nucleus, electron capture will replace a proton in the $f_{7/2}$ shell by a neutron in the unoccupied $f_{5/2}$ shell. In shell model language the capture is a transition to the allowed Gamow-Teller state. The strength of the capture reaction is then much larger than the experimentally determined strengths of β-decays (inverse electron captures) which, in going from the ground state to either a ground state or a low lying excited state, are inhibited. During stellar collapse the densities are large and electrons have sufficient (Fermi) energy to reach the $f_{5/2}$ shell. The neutron $f_{5/2}$ shell lies about 3 MeV above the ground state. The nucleus will thus be left with an excitation energy $\Delta_n \approx 3$ MeV following an electron capture. Describing the kinematics of the nucleons inside the nucleus by a Fermi gas model introduces at most a factor of 3 error in the capture rates (BBAL). Epstein and Pethick (1981) include thermal distributions for the electrons and neutrinos, as well as for the nucleons. The resulting finite temperature rates are larger than the zero temperature rates we use, but lead to a final lepton number only about 0.02 lower than when the $T = 0$ rates are used.

The mass number A, neutron number N, and proton number Z of the average nucleus all increase with increasing density and decreasing electron fraction. As collapse proceeds, the average nucleus becomes a less like an iron group nucleus. As has been recently pointed out by Fuller, Fowler, and Newman (1980; hereafter FFN), when the neutron number is 40 or more,[2] the final state neutron $f_{5/2}$ shell is full, and the allowed Gamow-Teller transition to that state does not occur. Instead the neutron must go to a g-level, which has opposite parity from the initial proton state. The matrix element for capture is then down by a factor $\sim 10^{-3}$ from the allowed transition. The capture rate is further inhibited by a higher threshold energy ($\sim$ 10 MeV versus 3 MeV). With these restrictions on the heavy capture rate, captures on outside protons dominate. We thus set the capture rate on heavy nuclei to zero whenever $N \geq 40$ (Fuller 1980). Along collapse trajectories with $s \approx 1.2$, this occurs for densities $\rho \gtrsim 10^{11}$ g cm^{-3}. Some collapse models were computed without this FFN restriction.

When the proton number exceeds 40 (or 38) and $N \leq 64$, heavy capture proceeds from the $g_{9/2}$ shell to the $g_{7/2}$ shell, and is once more an allowed transition. But for the neutron-rich nuclei present in the neutronized core $N > 64$ when $Z > 40$, so heavy capture remains forbidden. The proton number exceeds 40 only for densities in excess of 10^{13} g cm^{-3} where neutrinos are trapped and captures on outside protons (and neutrino absorptions on outside neutrons) easily maintain β-equilibrium.

Our equation of state is based on the approximation of one average heavy nucleus. We expect, however, that there will be an ensemble of heavy nuclei, as is seen in the many nuclear statistical equilibrium calculations in the literature. Our average nucleus describes only the peak of the distribution in A and Z. The single-nucleus approximation gives reasonable values for the baryon pressure

[2] When the neutron number is 38 or more if the $p_{1/2}$ shell lies above the $f_{5/2}$ shell.

© American Astronomical Society • Provided by the NASA Astrophysics Data System

1981ApJ...249..270V

(which is unimportant anyway), the nuclear binding energy, and the neutron and proton chemical potentials. Since there will be a number of nuclei with slightly different shell structures contributing to the heavy capture rate, any shell effects[3] in the individual rates will be averaged over, thus making the Fermi gas description more viable. The spread of nuclear masses cannot be ignored, however, when the neutron $f_{5/2}$ shell has just been closed (e.g., $N = 41$) in the average nucleus. The FFN restriction would then tell us that there are no electron captures on nuclei, even though there is a finite abundance of nuclei with $N < 40$ on which the captures can occur.

The capture rate on heavy nuclei was found by BBAL to be $\dot{Y}_e \equiv dY_e/dt = -X\rho Y_e{}^2 c\sigma_0/m_0$, where $\sigma_0 = 1.18 \times 10^{-44}$ cm^2, $m_0 = 1.659 \times 10^{-24}$ is the inverse of Avogadro's number,

$$X = \int_0^{\Delta_H} \frac{\epsilon_\nu{}^2}{m_e{}^2} d\epsilon_\nu \int^{\Delta_H - \epsilon_\nu} \frac{d\epsilon_p}{k_F{}^2/3m_p} \frac{3\epsilon_e{}^2}{\mu_e{}^3}, \quad (1)$$

$k_F c$ is the Fermi energy of the proton in the nucleus, and

$$\Delta_H = \mu_e - (\mu_n - \mu_p) - \Delta_n \equiv \mu_e - \hat{\mu} - \Delta_n \quad (2)$$

is the energy available in the reaction. Performing the integral in the above equation yields $X \propto \Delta_H{}^4$. The above is valid as long as there is no inhibition of the final states by a finite neutrino number density. With a finite neutrino density the energy available to capture becomes.

$$\Delta - \Delta_n = \mu_e - \hat{\mu} - \Delta_n - \mu_\nu \equiv \Delta - \Delta_n . \quad (3)$$

The capture rate on heavies is

$$\dot{Y}_{e,H} = -\frac{c\sigma_0 \rho Y_e}{4m_0 m_e{}^2 (k_F{}^2/3m_p)\mu_e{}^3} R_H = -6.0 \times 10^{-5} R_H \text{ s}^{-1}, \quad (4)$$

where

$$R_H = \left(X_H \frac{Z}{A}\right)\mu_e{}^2 \left\{\left(1 - F + \frac{F^2}{3}\right)[\Delta_H{}^4 - \mu_\nu{}^3(4\Delta_H - 3\mu_\nu)] + (1 - \tfrac{2}{3}F)[\tfrac{3}{5}\Delta_H{}^4 F - \mu_\nu{}^4(3F - \tfrac{12}{5}G)] + \tfrac{2}{15}\Delta_H{}^4 F^2 - \mu_\nu{}^4 G(\tfrac{4}{5}F - \tfrac{2}{3}G)\right\}, \quad (5)$$

$G = \mu_\nu/\mu_e$, and $F = \Delta_H/\mu_e$. We take 3 MeV for the excitation energy as long as there is that much energy available, i.e.,

$$\Delta_n = \min [[3 \text{ MeV}, \max \{0, \tfrac{1}{2}(\mu_e - \hat{\mu} - \mu_\nu)\}]] . \quad (6)$$

Note that when $\Delta_n < 3$ MeV there is insufficient energy to capture to the $f_{5/2}$ shell, and the use of the BBAL description overestimates the rate. We find $\Delta_n < 3$ MeV when $\rho < 3 \times 10^9$ g cm^{-3}, where little capture occurs on the dynamic time scale. The average energy of the emitted neutrino is found by taking the ratio of X to a similar integral containing an additional power of ϵ_ν in the integrand. This energy is then

$$\langle \epsilon_\nu \rangle_{H\text{-cap}} = \frac{3}{5}\frac{(X_H Z/A)\mu_e{}^2}{R_H}\{(1 - F + \tfrac{1}{3}F^2) \times [\Delta_H{}^5 - \mu_\nu{}^4(5\Delta_H - 4\mu_\nu)] + (1 - \tfrac{2}{3}F)[\tfrac{2}{3}F\Delta_H{}^5 - \mu_\nu{}^5(4F - \tfrac{10}{3}G)] + \tfrac{10}{63}\Delta_H{}^5 F^2 - \mu_\nu{}^5 G(\tfrac{11}{10}F - \tfrac{20}{21}G)\} . \quad (7)$$

ii) *Capture on Outside Protons*

The outside protons and neutrons are non-degenerate, nonrelativistic Fermi gases (except at high densities where the neutrinos are trapped and the weak interaction rates are so high that their exact formulae do not matter). Thus the proton phase space is not restricted by Fermi statistics, and the nucleon chemical potential difference, $\mu_n - \mu_p$, and the excitation energies, Δ_n and Δ_p, do not enter into the capture energy balance. For the phase space integral (analogous to eq. [1]) we do not integrate over the proton phase space. We neglect the neutron-proton mass difference and the recoil momentum of the nucleons, and set $\epsilon_\nu = \epsilon_e$. Proceeding as above, we obtain

$$\dot{Y}_{e,p} = -\frac{3c\sigma_0 \rho Y_e}{5m_0 m_e{}^2 \mu_e{}^3} R_p = -3.8 \times 10^{-3} R_p \text{ s}^{-1}, \quad (8)$$

where

$$R_p = Y_p(\mu_e{}^3 - \mu_\nu{}^3 G^2)\mu_e{}^2 . \quad (9)$$

Note that Y_p will always stand for the *outside* proton abundance. The average energy per emitted neutrino is

$$\langle \epsilon_\nu \rangle_{p\text{-cap}} = \frac{5(\mu_e{}^4 - \mu_\nu{}^4 G^2)}{6(\mu_e{}^3 - \mu_\nu{}^3 G^2)} . \quad (10)$$

We find that the outside proton abundance during the infall is large enough (typically $10^{-4} < Y_p < 10^{-3}$) that the capture rates on heavies and outside protons are comparable for densities less than 10^{11} g cm^{-3}. At higher densities the heavy capture rate, as given by equation (4), dominates.

In β-equilibrium, which is achieved when $\Delta = 0$, the net electron rate should be zero. For the heavy captures the rate does go to zero as β-equilibrium is approached. The capture rate on outside protons, on the other hand, does not. What is happening, of course, is that the reverse reaction of neutrino absorption, $\nu_e + n \rightarrow p + e^-$, becomes appreciable as the neutrino number density builds up, and, when equilibrium is attained, the electron capture rate is just balanced by the neutrino absorption rate.

Electron capture on outside protons and neutrino absorption on outside nucleons involve the same matrix element, so that the respective rates differ only by the nucleon abundances and the lepton phase space factors.

[3] If, for example, $21 \leq Z \leq 28$ and $34 \leq N \leq 40$, so that the capture transition is from the proton $f_{7/2}$ shell to the neutron $f_{5/2}$ shell, the matrix element should properly reflect the fraction of protons and neutron holes in the respctive shells: $|M_{GT}|^2 \approx (\frac{1}{7})(Z - 20)[(40 - N)/6]$. We do not include such shell effects in our heavy capture rates.

© American Astronomical Society • Provided by the NASA Astrophysics Data System

1981ApJ...249..270V

Neglecting the electron rest mass, setting $\epsilon_e = \epsilon_\nu$ as above, and substituting $x = \epsilon_e/T$, the rate for capture is

$$\lambda_{e^- + p \to n + \nu_e} = BY_p \int_0^\infty x^4 dx (e^{x - \mu_e/T} + 1)^{-1} \times (e^{\mu_\nu/T - x} + 1)^{-1}, \quad (11)$$

while the rate for absorption is

$$\lambda_{\nu_e + n \to e^- + p} = BY_n \int_0^\infty x^4 dx (e^{\mu_e/T - x} + 1)^{-1} \times (e^{x - \mu_\nu/T} + 1)^{-1}, \quad (12)$$

where we collect in B factors common to both rates. Note that here, unlike above, we do not approximate the Fermi factors, $(e^{x-\mu/T} + 1)^{-1}$, by step functions. The net rate of electron fraction change is

$$\dot{Y}_{e,p+n} = -\lambda_{e^- + p \to n + \nu_e}\left[1 - \frac{Y_n}{Y_p} e^{(\mu_\nu - \mu_e)/T}\right] = -\lambda_{e^- + p \to n + \nu_e}[1 - e^{(\mu_\nu + \hat{\mu} - \mu_e)/T}]. \quad (13)$$

In the last equality we have made use of the nondegenerate, nonrelativistic expressions for the nucleons. We thus multiply our outside proton capture rate by the factor $(1 - e^{\Delta/T})$. This serves to cut off the rate when β-equilibrium is approached, and allows for neutrino absorption whenever matter is shifted to the neutrino-rich side of β-equilibrium (which occurs upon expansion).

iii) *Total Rates*

The total rate of electron change is just $\dot{Y}_e = \dot{Y}_{e,H} + \dot{Y}_{e,p}$. We average the emitted neutrino energy from both types of capture by

$$\langle \epsilon_\nu \rangle_{\rm cap} = \frac{\langle \epsilon_\nu \rangle_{p\text{-cap}} \dot{Y}_{e,p} + \langle \epsilon_\nu \rangle_{H\text{-cap}} \dot{Y}_{e,H}}{\dot{Y}_{e,p} + \dot{Y}_{e,H}}. \quad (14)$$

Figure 1 shows the various energies involved in the electron capture rates, as well as the temperature, throughout a typical model when the central density has just reached 10^{14} g cm^{-3}. Figure 2 shows the ratio of the electron capture rate on protons to the electron capture rate on heavy nuclei, as a function of density. Both types of capture are comparable at the beginning of the collapse. The rate on nuclei dominates more as the density increases above 3×10^{10} g cm^{-3}, and would become 100 times more important than the proton rate (at $\rho \approx 6 \times 10^{11}$ g cm^{-3}) if the BBAL-like formula for heavy captures were used while $N \geq 40$. The dark points mark where $N = 40$, which occurs at a density $\rho \approx 10^{11}$ g cm^{-3}, where the rate on heavies is 4 times greater than the rate on protons. We also show the ratio for the complete trapping model. The out-of-whackness in this model is small, and there is little energy available to pay the excitation energy and neutron-proton chemical potential difference when capture occurs on nuclei, and the proton rate dominates in this case.

c) Neutrino Transport

The outcome of core collapse is sensitive to how quickly a neutrino, once created, moves through the matter. Neutrino interactions at low density ($\rho <$ few $\times 10^9$ g cm^{-3}) are rare enough that matter may be considered transparent to neutrinos. For densities in excess of 10^{12} to 10^{13} g cm^{-3} neutrino-baryon scattering is strong enough that the neutrinos are trapped, moving relative to the matter only by diffusion. Once such high densities are reached, the neutrinos quickly assume a Fermi distribution.

At intermediate densities, however, neither transparency nor diffusion is a valid assumption. Nor is it possible to assume a spectrum for the neutrinos in this regime, since the relevant cross sections are very energy dependent ($\propto \epsilon_\nu^2$). A proper treatment of these "photosphere" densities requires a multienergy group transport scheme. Such schemes are computationally costly and cumbersome. The aim of the present study, however, is to explore the effects of the equation of state on the collapse. We use, therefore, a relatively simple neutrino transport algorithm with which the calculation of a large number of collapse models is feasible. This leakage scheme does do quite well on the gross energetics of the neutrino transport and on the lepton distribution throughout the core as compared with recent detailed transport models of Wilson (1980*b*).

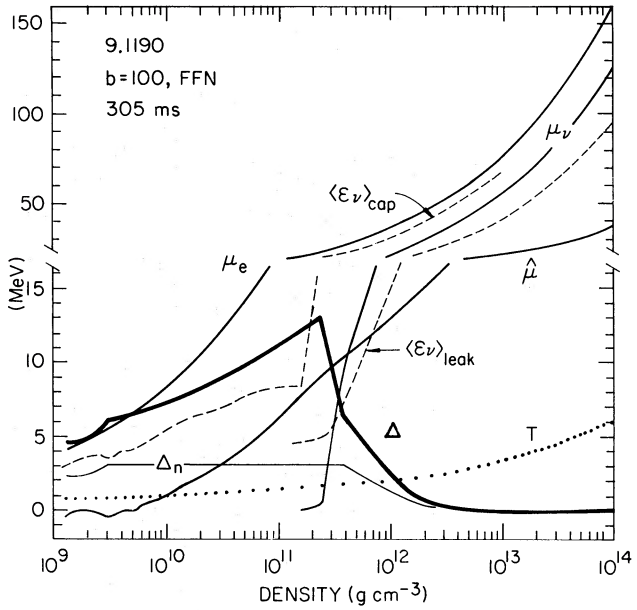

FIG. 1.—The several energies involved in electron capture, as a function of density through collapse model 9 (optical depth multiplier $b = 100$, electron capture on heavy nuclei restricted by the FFN criterion) when the central density $\rho_c = 10^{14}$ g cm^{-3}. The evolution with density of each mass shell in the core is similar. The chemical potentials of the electron and neutrino gases are μ_e and μ_ν, respectively. The difference of the nucleon chemical potentials is $\hat{\mu} = \mu_n - \mu_p$. The difference $\Delta = \mu_e - \hat{\mu} - \mu_\nu$ measures how far the matter is from β-equilibrium (or how much "out-of-whack"). The excitation energy of a heavy nucleus following electron capture, Δ_n, is given by eq. (6). The average energy of a neutrino resulting from the electron capture is $\langle \epsilon_\nu \rangle_{\rm cap}$, while the typical energy of a neutrino "leaking" from the neutrino sea is $\langle \epsilon_\nu \rangle_{\rm leak}$. Comparison of the lepton chemical potentials with the temperature, T, shows that both the electron and neutrinos are extremely degenerate.

© American Astronomical Society • Provided by the NASA Astrophysics Data System

1981ApJ...249..270V

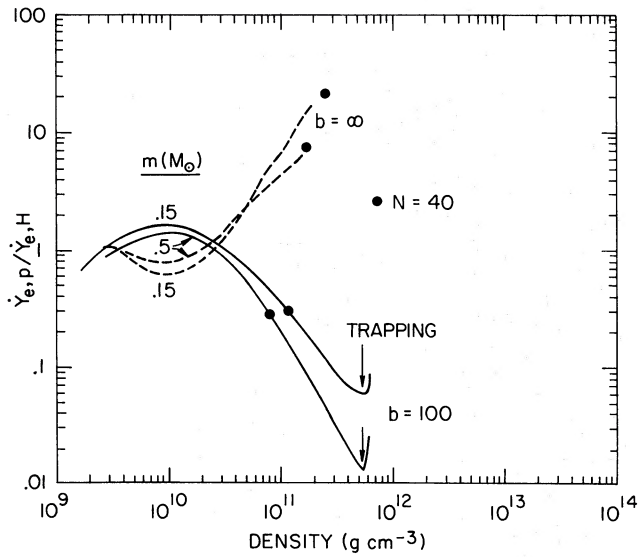

FIG. 2.—The ratio of the electron capture rate on outside protons to the capture rate on heavy nuclei, as a function of density during the collapse of mass shells $m = 0.15$ and $0.5\ M_\odot$. Captures on heavies dominate for points at the bottom of the graph. The dark points mark where the neutron number of the average heavy nucleus $N = 40$. At higher densities there is, according to FFN, virtually no electron capture on heavy nuclei. The solid curve shows the case for a neutrino trapping density $\rho_{trap} = 6 \times 10^{11}$ g cm^{-3}. Above the trapping density the buildup of the neutrino Fermi sea decreases the energy available for capture on heavies more than for captures on outside protons, and the latter reaction then dominates. The available energy is also small in the complete trapping model (*dashed line*), where the heavy rate is never dominant.

i) *Neutrino Leakage Scheme*

We approximate the transport of neutrinos by a leakage scheme—a fraction $\Delta t/t_\nu$ of any trapped neutrinos escape during an interval Δt. The leakage time is t_ν. Consider the speed with which neutrinos pass through a shell of matter, of thickness Δr, which has a mean free path for neutrinos λ. If the matter is transparent to neutrinos, i.e., if $\lambda/\Delta r \gg 1$, the neutrinos travel through the shell at the speed of light; the corresponding leakage time is $t_\nu = \Delta r/c$. In the diffusion limit, $\lambda/\Delta r \ll 1$, and the neutrinos random walk through the shell. The leakage time in this limit is $t_\nu = (b\Delta r^2/c\lambda)$, where b is a constant depending on the geometry of the system. In general, we would take for the leakage time from this shell

$$t_\nu = \Delta r(1 + b\Delta r/\lambda)/c\ , \tag{15}$$

which reproduces the above limits (this is similar to the approximations used in flux-limited diffusion).

Since the mean free path is not constant throughout the core, we replace $\Delta r/\lambda$ by the neutrino optical depth from the surface,

$$\tau(r) = \int_{R_8}^{r} dr/\lambda(r)\ , \tag{16}$$

where R_8 is the radius at $\rho = 10^8$ g cm^{-3}. Since $\Delta r/\lambda \ll 1$ for lower densities, the optical depth is insensitive to the choice of the lower limit on the integral. The leakage time is

$$t_\nu(r) = (R_8 - r)[1 + b\tau(r)]/c\ . \tag{17}$$

In a homogeneous star the leakage time, in the diffusion limit, is given by equation (15) with a value for b of order unity ($3/\pi^2$). In a star with a density gradient the average of $\Delta r/\lambda$ through the star is much less than in the homogeneous case, and a larger value of b is required in order to achieve the same leakage time at the same density. In addition, some elements of our leakage scheme, such as the choice of $\Delta r = R_8 - r$ and equation (20) below, are somewhat arbitrary. We therefore retain the optical depth multiplier b to "tune" the leakage time and achieve reasonable (as compared to other authors) trapping densities, ρ_{trap}, and final (at bounce) lepton fractions, $Y_{l,f}$. We consider several values of b both to account for uncertainties in the mean free path and to elucidate the sensitivity of the evolution to $Y_{l,f}$.

ii) *Mean Free Path*

The mean free path is usually dominated by coherent neutrino-nucleus scattering and elastic neutrino-nucleon scattering. The total mean free path is given by

$$\begin{aligned}\lambda_{\nu\text{-}N}^{-1} &= \frac{\rho\sigma_0\epsilon_\nu^2}{4m_0}\{a_p Y_p + a_n Y_n + [a_0 A + \tfrac{1}{2}a_1(Z-N)]^2 \\ &\quad \times Y_H + 16a_0^2 Y_\alpha\} \\ &= 1.63 \times 10^{-5}\left(\frac{\rho}{\mathrm{fm}^{-3}}\right)\left(\frac{\epsilon_\nu}{\mathrm{MeV}}\right)^2 \\ &\quad \times \{\tfrac{3}{4}Y_p + Y_n + [-\tfrac{1}{4}A + \tfrac{1}{4}(Z-N)]^2 Y_H + Y_\alpha\}\ ,\end{aligned} \tag{18}$$

where we have used $\sin^2\theta_W = 0.25$ for the Weinberg angle in the last equality. Ion-ion correlations, which we do not include, lower the coherent scattering cross section and increase the mean free path (Bond 1978). The correction is as large as a factor of 10 for densities $\rho \approx 10^{11}$ g cm^{-3}, where the largest decrease in Y_l takes place. The longer mean free path corresponds to a smaller optical depth multiplier b. When matter is dominated by α-particles (as it is in some postshock regions), neutrino-electron scattering is comparable to the nuclear scattering. We therefore included the contribution of neutrino-electron scattering whenever the expression in the curly brackets above was less than 1. The total mean free path in this case is given by $\lambda^{-1} = \lambda_{\nu-N}^{-1} + \lambda_{\nu-e}^{-1}$, where $\lambda_{\nu-e}$ is from Tubbs and Schramm (1975).

For each mass shell we use the average energy of a neutrino escaping from *that* shell in computing mean free path of that neutrino in all the overlying shells. In the transparent limit the escape energy is just the capture energy $\langle\epsilon_\nu\rangle_{cap}$. When neutrinos are leaking from a Fermi distribution of trapped neutrinos, the escape energy is $\frac{3}{4}\mu_\nu$. In general the average energy of an escaping neutrino is

$$\langle\epsilon_\nu\rangle_{escape} = W\langle\epsilon_\nu\rangle_{cap} + (1 - W)\langle\epsilon_\nu\rangle_{leak}\ , \tag{19}$$

where $\langle\epsilon_\nu\rangle_{leak} = \max\{\frac{3}{4}\mu_\nu, 3.15T\}$, and

$$W = \min\{1, 1\ \mathrm{s}/t_\nu\}\ . \tag{20}$$

© American Astronomical Society • Provided by the NASA Astrophysics Data System

1981ApJ...249..270V

The time constant, 1 s, in equation (20), although arbitrary, does not matter since changing that constant is equivalent to adjusting the optical depth multiplier. Our definition of $\langle \epsilon_\nu \rangle_{\rm leak}$ assumes an instantaneous downscatter of the emitted neutrino. (Epstein and Pethick 1981, who employ a time-dependent downscatter term, find no change when they vary the downscatter time scale by a factor of a hundred). In Figure 3 we show the radius r, mean free path λ, and W throughout the core of model 9, for which the optical depth multiplier $b = 100$. We also sketch W when $b = 1$.

The rate of electron fraction change, $\dot{Y}_e$, is given by the capture (and absorption) rates. The neutrino fraction changes by leakage, or by conversion of electrons via captures or absorption:

$$\dot{Y}_\nu = Y_\nu / t_\nu - \dot{Y}_e \, . \tag{21}$$

We treat ν_e, not $\bar{\nu}_e$, so $Y_\nu \geq 0$ always. The energy lost from the matter by neutrinos is

$$\dot{Q}_{\nu_e} = W \dot{Y}_e \langle \epsilon_\nu \rangle_{\rm cap} - (1 - W) Y_\nu \langle \epsilon_\nu \rangle_{\rm leak} / t_\nu \, . \tag{22}$$

The transport of muon (and tau) neutrino and antineutrino pairs was calculated similarly; these thermal neutrinos have no effect during the cool infall epoch.

In the leakage scheme neutrinos leaving some mass shell do not interact with any overlying matter. Our model thus has no neutrino energy or momentum deposition. While, with the luminosities we find, neutrino deposition would not itself eject matter, it would slow down (by momentum deposition) and heat (by energy deposition) the infalling matter at densities just below the photospheric density. A slower infall, if it results in a larger inner core at bounce, would lead to a stronger reflected shock. Lower preshock velocities, on the other hand, would weaken the shock. Energy deposition ahead of the shock would help the shock by presenting it with less tightly bound nuclei to break up, but the expansion of the heated preshock matter may reduce the preshock velocities. The net effect of deposition can only be addressed by a detailed transport calculation.

d) Hydrodynamics

The collapse model used explicit, general-relativistic (hereafter GR) hydrodynamics (see Van Riper 1979 for details), similar to the equations of May and White (1967). Some models were calculated using Newtonian hydrodynamics. The model was divided into 120 zones. Most infall models reported were calculated with this fixed zoning. A comparison model, continually rezoned to keep at least 10 shells per decade in density, showed no difference at all in the infall epoch. (Rezoning is important for following the shock propagation accurately.)

A quadratic von Neumann–Richtmyer artificial viscosity was used except during homologous infall. To the accuracy with which we could compute the entropy (due to the finite equation of state table) the artificial viscosity did not cause any anomalous increase in entropy. The first law of thermodynamics was solved iteratively, with the temperature as the independent variable.

III. INITIAL MODEL

Our initial model is the central 1.9 $M_\odot$ of the 15 $M_\odot$ evolutionary model of Weaver, Zimmerman, and Woosley (1978; hereafter WZW) shortly after collapse has commenced. (We emphasize that the model is collapsing and nothing artificial need be done to get it going.) Instability is due to the dissociation of iron nuclei. The central density, temperature, and electron fraction of this model are 6×10^9 g cm^{-3}, 0.72 MeV, and 0.427, respectively. The inner 1.5 $M_\odot$ is collapsing homologously (velocity $U \propto r$) with a maximum infall velocity of

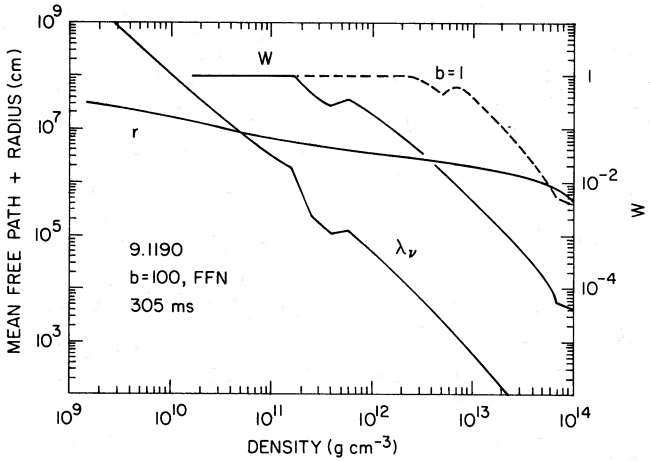

FIG. 3.—Profiles of the radius r, neutrino mean free path λ, and the transport quantity W, throughout the core of model 9, when the central density $\rho_c = 10^{14}$ g cm^{-3}. When $W = 1$, neutrinos escape freely, otherwise W is the inverse of the neutrino leakage time. A smaller optical depth multiplier, $b = 1$, results in the dashed curve.

© American Astronomical Society • Provided by the NASA Astrophysics Data System

1981ApJ...249..270V

-8.8×10^7 cm s^{-1} at $r = 1.6 \times 10^8$ cm. This homologous core coincides with the "iron" core (the silicon burning shell is located at $m = 1.55\ M_\odot$), which consists of iron group nuclei produced by silicon burning. Alphas are the second most dominant species, with a mass fraction $X_\alpha \approx 2 \times 10^{-2}$ for $m < 1\ M_\odot$, and rising to $X_\alpha = 0.1$ for $m > 1.1\ M_\odot$. The increase in the alpha abundance through the core is a reflection of the entropy distribution. The entropy per nucleon, calculated with our equation of state, rises from 1.16 at the center to 1.6 at $m = 1.1\ M_\odot$, and then increases to 2.5 for $m > 1.1\ M_\odot$.

The entropy distribution and the large mass of the iron core ($1.56\ M_\odot$ as compared to $M_{\rm Ch} = 1.25\ M_\odot$, the classical Chandrasekhar mass for $Y_e = 0.43$) are a consequence of the immediate precollapse evolution. Silicon burning first occurs in a central convective region, extending to $m \approx 1\ M_\odot$, for about 5.2×10^5 seconds. Electron captures during this epoch reduce both the entropy and electron fraction. The density dependence of the capture rates accounts for the slight gradient in these quantities for $m < 1\ M_\odot$. Hydrostatic core burning is followed by a silicon shell flash. Matter overlying the iron core both expands and burns to iron. Upon contraction the core mass is greater than $1.5\ M_\odot$ and dynamic collapse ensues. That the core mass exceeds the Chandrasekhar mass is a consequence of dynamic evolution rather than quasi-static growth pushing an iron core over the edge. The extent of the convective region associated with the shell burning is marked by the plateau with $Y_e \approx 0.48$ between 1.1 and $1.5\ M_\odot$. The silicon burning in the outer layers has increased the entropy there, and since collapse immediately follows the flash, neutrino emission has not reduced it much by the time of our initial model.

We construct our initial model from the WZW data by taking directly their density, pressure, electron fraction, and velocity as a function of rest mass. Our temperature was then chosen to be consistent with these data, as was the radius. Because of the different equations of state the temperatures differed by a few percent (e.g., we found $T = 0.79$ MeV at the center compared with their 0.72 MeV). (We did not have values for their entropy.) Our α-particle abundance was higher throughout the core: $X_\alpha = 0.07$ versus 0.01 at the center and 0.2 versus 0.1 at the peak in X_α at $m = 1.2\ M_\odot$. Our higher α-particle abundance may mean a lower average adiabatic index (by being further into the phase transition), but we do not know WZW's value for $\langle\Gamma\rangle$. Our free neutron abundance was lower by a factor of 2. The free proton abundances agreed for $Y_p \geq 10^{-3}$. Our model extended beyond the iron core to $m = 1.89\ M_\odot$, thus ensuring that our choice of boundary condition would not affect the core evolution. The average of the adiabatic index over the entire $1.89\ M_\odot$ model was

$$\langle\Gamma\rangle = \int \Gamma P dV \Big/ \int P dV = 1.304\ .$$

This average, which includes contributions from $\Gamma \gtrsim \frac{4}{3}$ matter beyond the homologous core, overestimates $\langle\Gamma\rangle$ in the collapsing core.

The mass number of our heavy nucleus varied between $A_H = 60$ at the center and $A_H = 50$ at $m = 1.2\ M_\odot$, while the proton number was $Z_H \approx 25$ throughout the core. The matter was out of β-equilibrium by between 3.5 and 4.5 MeV. The neutrino energy loss rates were dominated by electron capture neutrinos, for which $\dot{Q}_c = 10^{17}$ ergs g^{-1} s^{-1}, much larger than the thermal emissivity $\dot{Q}_t = 2 \times 10^{13}$ ergs g^{-1} s^{-1} of ν_μ, $\bar{\nu}_\mu$ and ν_τ, $\bar{\nu}_\tau$ pairs. The total neutrino luminosities were 5×10^{49} ergs s^{-1} for the capture neutrinos and 10^{47} ergs s^{-1} for the thermal neutrinos, with average energies per neutrino of 2.7 and 6.5 MeV, respectively.

IV. INFALL EPOCH

a) *Evolutionary Models*

In this paper we report on evolution between the initial model and when the collapsing core attains a central density $\rho_c = 10^{14}$ g cm^{-3}. Our results on core bounce, shock formation, and propagation are elsewhere. We summarize in this paragraph the features which we varied from model to model. The neutrino optical depth is multiplied by the parameter b (eq. [16]); for small b, neutrinos are trapped only at high density. *Complete trapping*, where neutrinos can be created or absorbed, but never escape, corresponds to $b = \infty$ (in the calculations we set $\infty = 10^{100}$). In the *adiabatic* models the electron fraction did not change. General-relativistic hydrodynamics was employed in most of the models; several used the Newtonian limit. According to Fuller, Fowler, and Newman (FFN), electron capture on heavy nuclei is severely suppressed for $N \geq 40$; FFN denoted a model obeyed this rule. Electrons can be captured by either heavy nuclei (H-cap) or by outside protons outside the nuclei (p-cap). We occasionally turn off one of these channels. In one model we set the nuclear excitation emergy, Δ_n, to zero. Table 1 lists the combinations actually used, together with some results.

Model 9 is typical. Captures on heavy nuclei were cut off à la FFN, and, with an optical depth multiplier $b = 100$, neutrinos were trapped for $\rho > 1.6 \times 10^{11}$ g cm^{-3}, resulting in $Y_{l,f} = 0.36$. The latest calculations of Wilson with the FFN cutoff find $Y_{l,f} \approx 0.4$ (Wilson 1980*b*). Figure 4 shows profiles of density, entropy, velocity, and lepton and neutrino fractions for several times during the collapse, including the initial model (curve 0). The sharpness of the transition to neutrino trapping is evident in the lepton fraction profiles. Figure 5 shows two infall adiabats (taken from the adiabatic model) in temperature-density space, as well as the trajectories for our lowest and highest entropy collapses.

b) *Equation of State*

Figure 6 shows the composition for three mass shells, with $m = 0.15$, 0.3, and $0.5\ M_\odot$, during the collapse of model 9. These three shells differ slightly in entropy (see Fig. 4*b*). Also shown (*dashed line*) is the composition for $m = 0.15\ M_\odot$, from a high entropy collapse, for which $s = 1.92$ when $\rho > 10^{12}$ g cm^{-3}. The heavy nuclei, with

© American Astronomical Society • Provided by the NASA Astrophysics Data System

© American Astronomical Society • Provided by the NASA Astrophysics Data System

TABLE 1

COLLAPSE RESULTS

MODEL					ρ_c[a]																
	X = ON				=1+14				U_{min}												
	FFN	GR		b	or	t (ms)	$m_{u_{min}}$[b]	M_{GW}[c]	m_{sonic}	(10^9 cm/s)	M	ρ	Y_ℓ	Y_e	d	d_y	Δs[d]	X	Δ_{max} (MeV)	$\rho(\Delta_{max})$	ρ_{40}	ρ_{trap}	ρ_β
7	X	X		10		304.2	.61	.60	.41	-3.4	.15	4.0+13	.341	.284	.51	.61	-.21	3.5	14.5	4.0+11	8.0+10	4.0+11	5.0+12
											.50	3.0+12	.328	.297	.53	.59	-.15	1.4	17.5	6.0+11	1.2+11	6.5+11	>3.0+12
8	X	X		1		303.8	.43	.50	.32	-3.4	.15	3.5+13	.310	.264	.45	.54	-.54	3.4	26.5	2.0+12	8.0+10	2.0+12	5.0+12
											.50	1.2+12	.262	.262	.58	.49	-.04	1.6	>24.0	>1.2+12	1.2+11	>1.2+12	>1.2+12
9	X	X		100		304.8	.71	.66	.47	-3.5	.15	4.0+13	.357	.292	.54	.63	-.02	3.8	10.0	1.6+11	8.0+10	1.6+11	2.0+12
											.50	5.0+12	.350	.301	.55	.62	+.01	1.3	12.0	2.0+11	1.2+11	2.3+11	2.0+12
10		X	no H-cap	10		314.8	.69	.63	.45	-3.4	.15	4.0+13	.365	.298	.53	.65	-.37	3.7	16.5	4.0+11	1.0+11	4.0+11	1.3+13
											.50	4.5+12	.354	.317	.55	.65	-.40	1.6	19.0	5.5+11	2.7+11	6.0+11	>4.5+12
11	X	X	no p-cap	10	4.5+13	315.0	.55	.63	.40	-3.1	.15	2.0+13	.258	.223	.53	.43	+.74	3.5	26.0	2.2+12	1.0+11	2.2+12	1.3+13
											.50	1.2+12	.263	.263	.58	.49	+.76	1.0	>21.0	>1.2+12	2.0+11	>1.2+12	>1.2+12
12		X	no p-cap	10	1.0+12	308.4	.53	.69	1.4	-0.87	.15	6.0+11	.255	.255	.56	.48	+.70	3.7	>11.0	>6.0+11	1.2+11	>6.0+11	>6.0+11
											.50	8.0+10	.392	.392	.81	.84	+.18	3.2	>10.0	>8.0+10	>8.0+10	>8.0+10	>8.0+10
13		X		10	2.2+12	298.4	.75	.65	>1.4	-0.85	.15	6.0+11	.257	.257	.54	.48	+.47	3.4	>11.0	>6.0+11	8.0+10	>6.0+11	>6.0+11
											.50	8.0+10	.383	.383	.77	.81	+.05	3.0	>9.0	>8.0+10	>8.0+10	>8.0+10	>8.0+10
14		X	Adiabatic			352.8	1.18	1.31	.91	-3.2	.15	5.0+13	.432	.432	.86	1.00	0	5.3	135.0	5.0+13	3.0+12		
											.50	1.3+13	.447	.447	.87	1.00	0	3.4	95.0	1.3+13	6.0+12		
15	X	X		∞		274.5	1.03	.84	.69	-3.6	.15	4.0+13	.432	.337	.64	.78	+.08	4.5	4.0	5.0+9	2.0+11		2.0+11
											.50	1.1+13	.447	.348	.65	.78	+.09	2.8	4.5	3.0+9	3.0+11		2.0+11
16	X			20		365.2	.73	.61	.53	-3.7	.15	4.5+13	.350	.285	.52	.61	-.14	4.2	12.0	2.5+11	8.0+10	2.5+11	5.0+12
											.50	7.0+12	.337	.291	.52	.59	-.15	1.8	14.5	3.5+11	1.2+11	4.0+11	5.0+12
19			Adiabatic			447.5	1.31	1.31	1.12	-3.4	.15	5.5+13	.432	.432	.86	1.00	0	7.6	140.0	5.5+13	3.0+12		
											.50	2.0+13	.447	.447	.86	1.00	0	5.0	116.0	2.0+13	6.0+12		
20	X	X	{no p-cap, $\Delta_n = 0$}	10		254.1	.65	.63	.43	-3.7	.15	4.0+13	.332	.274	.53	.58	+.28	3.6	28.0	1.5+12	6.0+10	1.5+12	1.0+13
											.50	5.0+12	.280	.275	.56	.52	+.44	1.8	29.5	2.5+12	1.0+11	4.0+12	>5.0+12
22	X			10		365.0	.68	.59	.49	-3.6	.15	4.0+13	.341	.284	.50	.61	-.21	4.1	14.5	4.0+11	8.0+10	4.0+11	5.0+12
											.50	5.5+12	.328	.287	.51	.57	-.21	1.5	17.0	6.0+11	1.2+11	6.5+11	6.0+12
23	X			100		365.7	.78	.66	.57	-3.7	.15	4.0+13	.357	.292	.54	.63	-.04	4.5	10.0	1.6+11	8.0+10	1.6+11	2.0+12
											.50	8.0+12	.350	.296	.54	.61	-.01	2.2	12.0	2.0+11	1.2+11	2.0+11	2.0+12
24				10	2.2+12	358.7	.60	.55	>1.4	-0.88	.15	6.0+11	.255	.255	.53	.47	+.48	3.7	>11.0	>6.0+11	8.0+10	>6.0+11	>6.0+11
											.50	9.0+10	.380	.380	.75	.81	+.05	3.0	>9.0	>9.0+10	>9.0+10	>9.0+10	>9.0+10
25	X	X		1000		302.5	.87	.76	.60	-3.5	.15	5.5+13	.411	.322	.60	.74	-.07	4.2	6.5	2.8+10	1.0+11	2.8+10	7.0+11
											.50	1.3+13	.402	.324	.58	.70	-.04	2.2	8.3	5.0+10	1.3+11	5.0+10	7.0+11
30		X		100		295.0	.49	.56	.35	-3.7	.15	4.0+13	.265	.240	.49	.47	+.28	3.2	10.5	5.5+11	7.0+10	6.0+11	7.0+11
											.50	6.0+11	.272	.270	.54	.51	+.40	1.0	14.0	6.0+11	1.0+11	5.0+11	9.0+11
32	X			1000	1.2+14	369.4	.98	.76	.77	-4.2	.15	6.0+13	.411	.322	.60	.74	-.07		6.0	2.8+10	9.0+10	2.8+10	7.0+11
											.50	2.0+13	.403	.320	.58	.69	-.04		8.0	5.0+10	1.3+11	5.0+10	7.0+11

a) All densities in g cm^{-3}.
b) All masses in $M_\odot$.
c) Calculated using d (m = .15 $M_\odot$).
d) S_i = 1.18 (1.30) for m = .15 (.50)

1981ApJ...249..270V

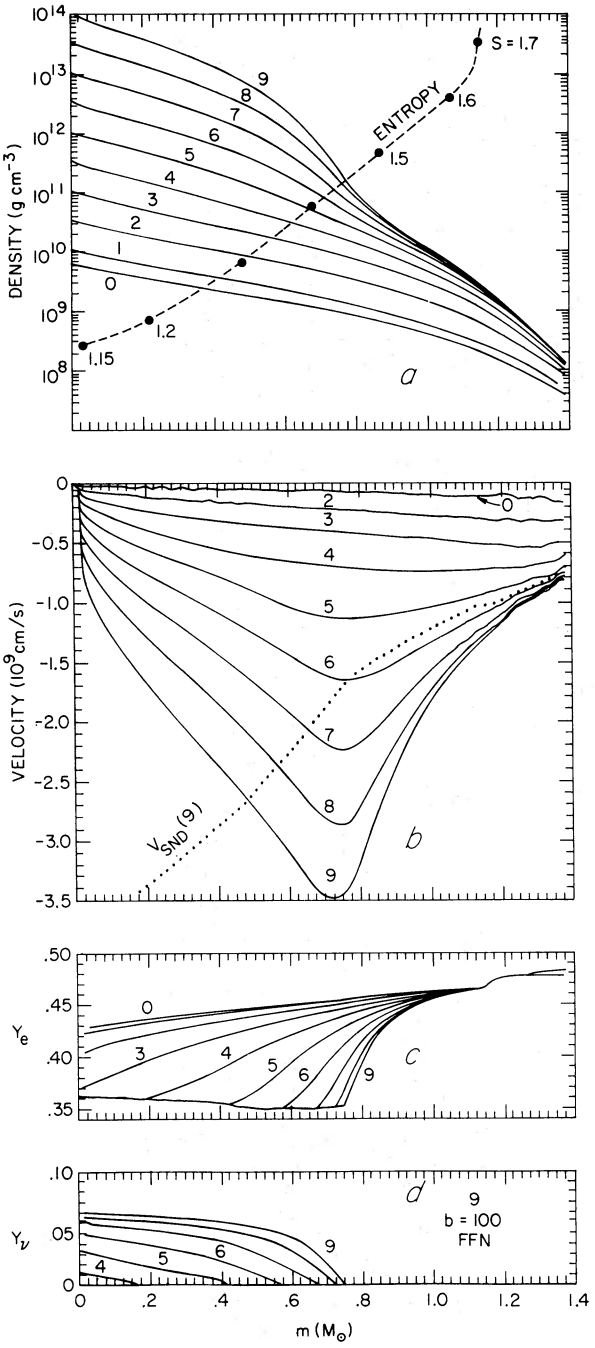

FIG. 4.—Instantaneous profiles of density and entropy (*dashed line*) (*a*), velocity (*b*), and lepton (*c*) and neutrino fractions (*d*), for several times during the infall of model 9. The same models are plotted in each graph. We only show one curve for the entropy, which is nearly constant during the infall. The full set of entropy profiles lie within $\Delta s = 0.05$ of the line shown.

$X_H \approx 0.9$, dominate the baryon composition during the entire infall. The heavy fraction decreases to $X_H \approx 0.7$ in the high entropy model. For densities below 10^{10} g cm^{-3}, α-particles are the second most dominant species, with $X_\alpha \approx 0.1$, while above 10^{11} g cm^{-3} outside neutrons, with $X_n \approx 0.1$, dominate the α-particles. The outside proton abundances are between 10^{-4} and 10^{-3}. The increase in the neutron fraction and the concurrent decrease in the α-particle and proton abundances are due mostly to the neutronization of the matter (i.e., decreasing Y_e). At constant entropy and constant electron fraction the outside nucleon abundances increase with density. The increase in the proton fraction for densities above 10^{12} g cm^{-3} is due to this general trend. For $Y_e = 0.43$ and $s = 1.2$ we find $X_n \approx 0.02$ and $X_p \approx 0.01$ at 7×10^{13} g cm^{-3}. The neutron, proton, and α-particle abundances all increase with entropy. The neutron fraction becomes as large as $X_n = 0.3$ for the high entropy model. The proton and α-particle abundances are sensitive to the electron fraction. The proton fractions at 7×10^{13} g cm^{-3} and $m = 0.15\ M_\odot$ are 2×10^{-4}, 10^{-3} 3×10^{-3}, and 10^{-2} for electron fractions of 0.28, 0.29, 0.34, and 0.43, respectively. Similarly, the α-particle abundances are 3×10^{-3}, 4×10^{-4}, 10^{-2}, and 2×10^{-2}. The variations in the larger neutron fraction are much less, varying between $X_n = 0.07$ and 0.1. The small differences in entropy among the models are as important as the differences in the electron fraction for the neutron abundance.

Once β-equilibrium obtains, the chemical potentials satisfy $\mu_e - \mu_\nu = \mu_n - \mu_p \equiv \hat{\mu}$. The electron and neutrino chemical potentials, μ_e (= 160 MeV at $\rho = 10^{14}$ g cm^{-3} and $Y_l = 0.36$) and μ_ν (120 MeV), are both much larger than $\hat{\mu}$ (40 MeV). It is tempting to approximate this situation by $\hat{\mu} = 0$ and $\mu_e = \mu_\nu$. This implies, since both lepton gases are extremely degenerate and relativistic, that $Y_e = 2Y_\nu$ or $Y_e = \frac{2}{3}Y_l$. Inspection of Table 1 shows that this underestimates the electron fraction by 15% for $Y_l = 0.432$ (model 15) and by 36% for $Y_l = 0.265$ (model 30). For smaller Y_l both of the lepton chemical potentials are smaller, and the neglect of $\hat{\mu}$ matters more.

c) *Heavy Nucleus*

The mass number A, neutron number N, and proton number Z of the heavy nucleus are shown in Figure 7, as a function of density for mass shell $m = 0.15\ M_\odot$. These curves are nearly the same for the slightly higher entropies of shells 0.3 and 0.5 $M_\odot$. We also show the results for two models with higher entropies, and for the adiabatic model (*light curve*), in which Y_e remains constant. At low density the heavy nuclei, with $A \approx 60$ and $Z \approx 25$, are much like iron peak nuclei. All three quantities increase with density (as long as the entropy is not too large) and with decreasing electron fraction. The mass number becomes as large as 1000 at 10^{14} g cm^{-3}. The nuclei become more neutron-rich as they get larger. The increased mass number for smaller Y_e is due mostly to the addition of neutrons.

According to FFN the electron capture rate on heavy nuclei is strongly suppressed when $N \geq 40$. We denote

© American Astronomical Society • Provided by the NASA Astrophysics Data System

1981ApJ...249..270V

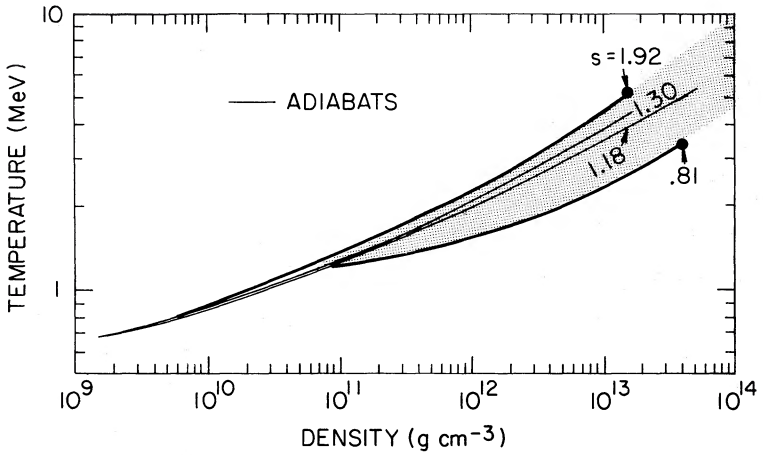

FIG. 5.—All of the infall trajectories of the models considered lie within the shaded region, which is bounded by the trajectories of the highest and lowest entropy collapses calculated. The two curves in the center are adiabats with $s = 1.30$ ($m = 0.5\ M_\odot$) and $s = 1.18$ ($0.15\ M_\odot$).

the density when $N = 40$ by ρ_{40}. For numerical reasons[4] the onset of this restriction was smoothed out, and there was a finite capture rate on heavy nuclei even when N was slightly greater than 40. This very crudely approximates the situation when an ensemble, rather than just one species, of heavy nuclei is present.

d) Neutrino Trapping Density

The trapping density $\rho_{\rm trap}$, beyond which the neutrino fraction is finite, is, in our models, most sensitive to the optical depth multiplier b. Figure 8 shows the total lepton fraction Y_l, and the neutrino fraction Y_ν, as a function of density for the shell $m = 0.15\ M_\odot$, for several models with b between 1 and ∞. (The latter value of b corresponds to complete trapping.) The heavy capture rates were restricted by the FFN criterion in these models. The lepton fraction decreases with increasing density until $\rho = \rho_{\rm trap}$. At higher densities all neutrinos from electron captures remain in the matter and the lepton fraction does not change with density. The sharp onset of Y_l = constant occurs because the neutrino mean free path λ decreases rapidly with increasing density and because matter quickly passes through the trapping density (on a dynamical time scale). For higher trapping densities more neutrinos can escape (Fig. 3), resulting in lower lepton fractions, larger pressure deficits, less massive inner cores, and, ultimately, weaker shock waves. Other collapse models with more detailed neutrino transport (Wilson 1980*b*; Arnett 1977*b*), find $\rho_{\rm trap} \approx$ few $\times\ 10^{11}$ g cm^{-3}, corresponding to our models with $b = 100$ ($\rho_{\rm trap} = 1.6 \times 10^{11}$ g cm^{-3}) and $b = 10$ (4×10^{11} g cm^{-3}). Our trapping density also depends on assumptions about the electron captures (see § V*e* below).

Figure 9 shows the out-of-whackness, $\Delta = \mu_e - \hat{\mu} - \mu_\nu$, for the same models as in Figure 8. This, minus the neutron excitation energy, Δ_n, is the energy available to drive electron capture on nuclei (capture on outside protons does have to pay $\hat{\mu}$ or Δ_n). The out-of-whackness increases with density until it peaks at the trapping density, becoming as large as 27 MeV when $\rho_{\rm trap} \approx 2 \times 10^{12}$ g cm^{-3}. For higher densities the neutrino number, and hence the neutrino chemical potential,

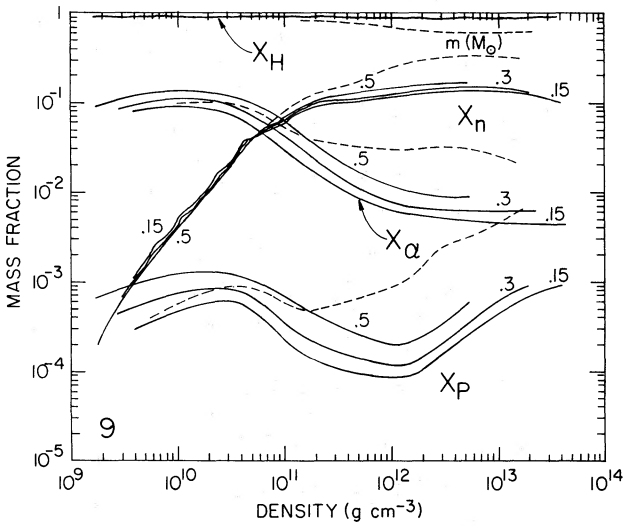

FIG. 6.—The abundance, by mass, of heavy nuclei (H), alpha particles (α), and outside (or free) neutrons (n) and protons (p) for three mass shells during the collapse of model 9. The mass shells shown are $m = 0.15$, 0.3, and $0.5\ M_\odot$. The outermost shells have a slightly higher entropy, and hence a greater abundance of alpha particles and free nucleons. Also shown are the abundances, for $m = 0.15\ M_\odot$, for a high entropy collapse (*dashed line*). The entropy $s = 1.92$ for $\rho \gtrsim 10^{12}$ g cm^{-3}, while $1.2 \leq s \leq 1.4$ along the solid curves.

[4] We tabulated $X_Z = (Z/A)X_H$, the mass fraction of protons in nuclei, at each point in our equation of state table. If the FFN criterion was met at a grid point, we entered zero instead. Since there were some points with $X_Z \neq 0$ at the corners of the interpolation cell a finite capture rate on heavies was calculated, even though we later find $N > 40$ at that point. Machine memory limitations made the inclusion of another entry (namely N) in the equation of state table infeasible.

© American Astronomical Society • Provided by the NASA Astrophysics Data System

1981ApJ...249..270V

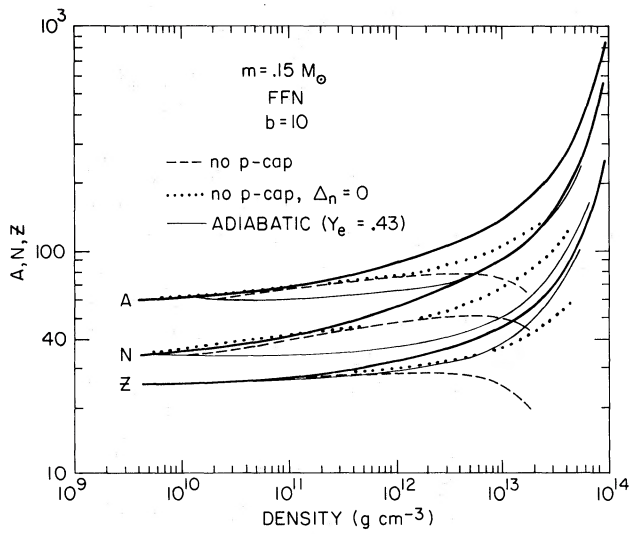

FIG. 7.

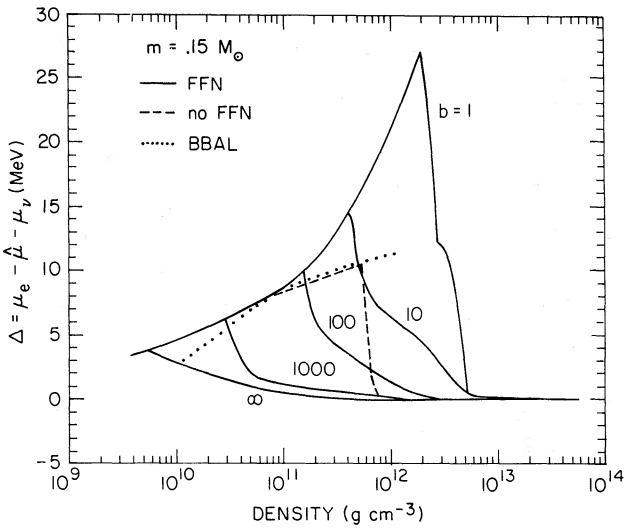

FIG. 9.

FIG. 7.—The mass number A, neutron number N, and proton number Z, as a function of density for mass shell $m = 0.15\ M_\odot$ for several collapse models. The light solid curves are from the adiabatic model, where Y_e (= 0.43) remain constant. Electron capture on outside protons was not included in the models shown by the dashed lines; as a result these models evolve to higher entropies ($s = 1.92$ for $\rho > 10^{12}$ g cm^{-3}) than the standard model (*solid dark line* for which $s \approx 1.2$). The dotted line shows the results when the excitation energy of the heavy nucleus following electron capture, Δ_n, is set to zero.

FIG. 9.—The "out-of-whackness," $\Delta = \mu_e + \mu_p - \mu_n - \mu_\nu = \mu_e - \hat{\mu} - \mu_\nu$, as a function of density at mass shell $m = 0.15\ M_\odot$. For larger m, $\Delta(\rho)$ is only slightly higher. The curves are labelled by the value of the optical depth multiplier, b. The solid curves were calculated with the FFN restriction on electron capture on heavy nuclei. The dashed line was computed without this restriction. The case $b = \infty$ corresponds to complete trapping, where no neutrinos can escape. The dotted line is from BBAL, Table 10.

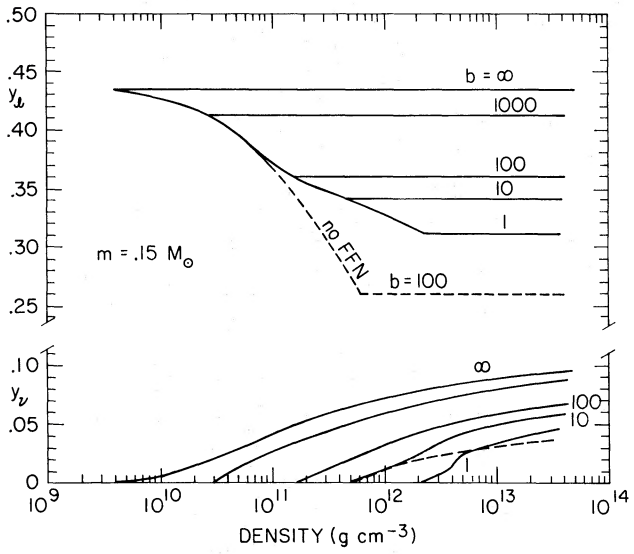

FIG. 8.—The total lepton fraction $Y_l = Y_e + Y_\nu$ (*top curves*) and the neutrino fraction Y_ν (*bottom curves*), as a function of density at mass shell $m = 0.15\ M_\odot$. The curves are labeled by the value of the optical depth multiplier, b. The solid curves were calculated with the FFN restriction on electron capture on heavy nuclei; the dashed line was computed without it. The case $b = \infty$ corresponds to complete trapping, where no neutrino can escape.

increase with density, thus reducing Δ. When $\Delta = 0$, β-equilibrium obtains. For trapping densities $\rho_{\rm trap} \approx$ few $\times\ 10^{11}$ g cm^{-3}, β-equilibrium is not achieved until 10 times the trapping density in the FFN restricted models. The slowing down of the decrease of Δ with increasing density for $\rho > 5 \times 10^{11}$ g cm^{-3} is due to the decreasing free proton abundance (see Fig. 6).

The magnitude of Δ is due to the competition between the collapse rate, which determines primarily how fast μ_e increases, and the capture rate, which determines how fast μ_e decreases and, if the neutrinos are trapped, how fast μ_ν increases. Without the FFN restriction the capture rates are approximately 100 times faster, and β-equilibrium obtains shortly after trapping (dashed line in Fig. 9). We also show the result of BBAL, who find that Δ is no more than 2 MeV lower than ours (dotted line in Fig. 9; this curve should be compared to our models without the FFN restriction). In Table 1 we give the trapping density, $\rho_{\rm trap}$, and the density, $\rho_{\rm equil}$, where β-equilibrium first obtains, for mass shells $m = 0.15\ M_\odot$ and $0.5\ M_\odot$. Both of these densities increase slightly with mass due to the increase of the collapse rate with m and to the steeper density gradient in the outer layers of the core.

e) Electron Capture Rates

We have calculated a number of models to explore the effects of FFN restriction and the importance of captures on outside protons. With one exception (model 11), lower capture rates lead to a higher final lepton fraction, a larger out-of-whackness, and a larger ratio of the density where β-equilibrium first obtains to the trapping density. The

© American Astronomical Society • Provided by the NASA Astrophysics Data System

1981ApJ...249..270V

effect of the FFN restriction is apparent in the behavior of Y_l with density (Fig. 8). Above $\rho_{40} \approx 10^{11}$ g cm^{-3}, captures on heavier no longer contribute, and the decrease of Y_e ($= Y_l$ before trapping) with density slows down (*solid curves*). Without the FFN restriction (*dashed curve*), Y_e decreases faster as the density increases. The difference in the final lepton fraction is nearly 0.1 for models with the same optical depth multiplier b ($= 100$). The trapping density is greater for the nonrestricted model than for a restricted model which has the same value of b. This difference is due to the average energy of the capture neutrinos from which we compute the neutrino mean free path. In the restricted model, capture occurs only on outside protons for $\rho > \rho_{40}$, resulting in an average neutrino energy (while $\mu_\nu = 0$) $\langle \epsilon_\nu \rangle_{p\text{-cap}} = \frac{5}{6}\mu_e$. In the unrestricted model heavy captures dominate, so that

$$\langle \epsilon_\nu \rangle_{H\text{-cap}} = \tfrac{3}{5}(\mu_e - \hat{\mu} - \Delta_n) < \langle \epsilon_\nu \rangle_{p\text{-cap}} .$$

In addition, the greater rate of capture in the unrestricted model has prevented the out-of-whackness from becoming as large as in the restricted model, thereby increasing even further the difference in the neutrino energies. With less energetic neutrinos the mean free path is greater, and higher densities are required for trapping. Once trapping prevails ($\rho_{\rm trap} = 6 \times 10^{11}$ g cm^{-3} for the unrestricted model shown in Figs. 8 and 9), the high unrestricted capture rates quickly bring about β-equilibrium ($\rho_{\rm equil} = 7 \times 10^{11}$ g cm^{-3}).

We show the lepton and neutrino fractions in Figure 10, and the out-of-whackness in Figure 11, as a function of density for mass shell $m = 0.15\ M_\odot$, for various assumptions about the capture rate. For densities below

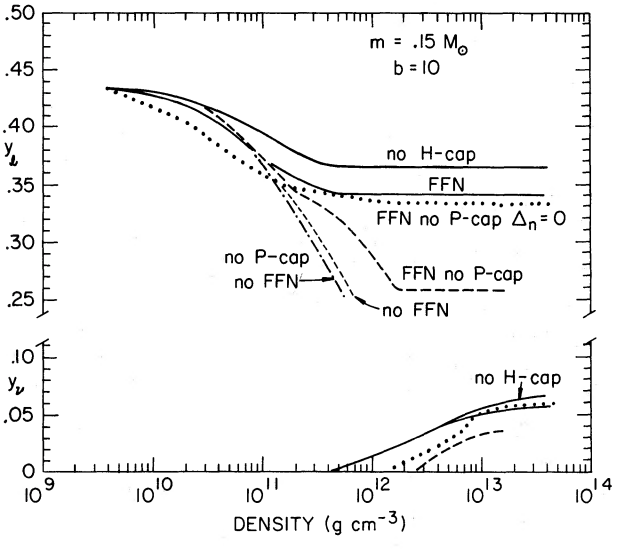

FIG. 10.—The total lepton fraction $Y_l = Y_e + Y_\nu$ and the neutrino fraction Y_ν, as a function of density at mass shell $m = 0.15\ M_\odot$. The optical depth multiplier $b = 10$ for all the models shown. The label "FFN" means the FFN restriction on heavy captures was obeyed. The electron capture rate on outside protons (heavy nuclei) was set to zero for the cases labeled "no p-cap" ("no H-cap"). The nuclear excitation energy per electron capture, Δ_n, which was set to zero in one of the models illustrated (*dotted line*), is otherwise given by eq. (6).

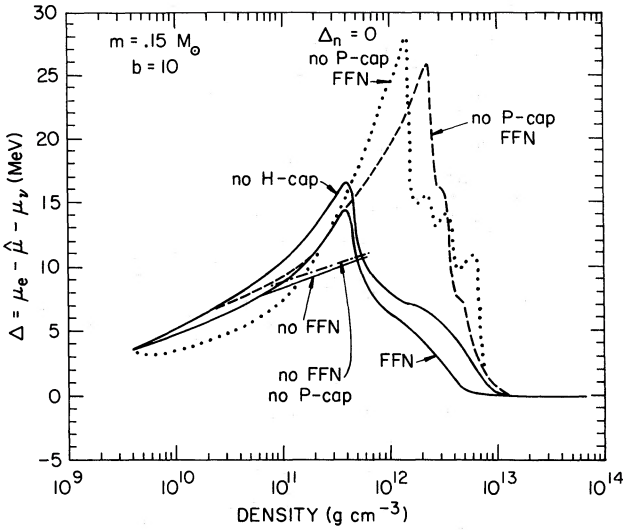

FIG. 11.—The "out-of-whackness", $\Delta = \mu_e + \mu_p - \mu_n - \mu_\nu = \mu_e - \hat{\mu} - \mu_\nu$, as a function of density at mass shell $m = 0.15\ M_\odot$. For larger m, $\Delta(\rho)$ is slightly higher. The same cases are displayed as in Fig. 10.

$\rho_{40} \approx 10^{11}$ g cm^{-3}, captures on outside protons and on heavy nuclei are comparable; above ρ_{40} only the outside proton rate contributes in the restricted models. A model computed without the heavy contribution[5] (denoted by "H-cap") at all densities is therefore not very different from a standard model with the FFN restriction. The lepton fraction does not decrease as fast as in the standard model, and the final Y_l is higher by 0.025. The model without heavy captures is more out of whack by at most 2 MeV before trapping, which occurs at the same density as in the standard model with the same value of b. Since the captures occur solely on protons, the entropy is lower than in the standard model, resulting in lower outside proton abundances and a higher equilibrium density.

Because of their low abundance ($10^{-4} \leq X_p \leq 10^{-3}$), the density of outside protons is not constrained by the overall requirements of mass ($X_H + X_\alpha + X_n + X_p = 1$) and charge ($Y_e = Z_H X_H + \frac{1}{2}X_\alpha + X_p$) balance. The density of the nondegenerate proton gas varies exponentially with the chemical potential, so the proton abundance is sensitive to the nuclear model used in the equation of state. Arnett (1977*b*), for example, finds Y_p a thousand times lower than ours. We have run some models taking the limit of no outside protons at all,[6] and hence no electron captures on protons (denoted by "no p-cap"). At the beginning of collapse ($\rho < 6 \times 10^{10}$ g cm^{-3}) the models without proton capture have a higher lepton fraction and a larger out-of-whackness, as do the models without heavy capture, than the standard model with both types of electron capture. A model without the FFN restriction on heavy capture and without proton capture remains more out-of-whack by $\frac{1}{2}$ MeV, but evolves to a

[5] We changed only the capture rates, not the equation of state.

[6] See no. 5.

© American Astronomical Society • Provided by the NASA Astrophysics Data System

1981ApJ...249..270V

lower lepton fraction (Y_l differs by 0.015 at 4×10^{11} g cm^{-3}) than the corresponding standard model. Because the initial lepton loss is less the pressure deficit is not as great, and the model without proton captures is collapsing more slowly through the densities between 10^{10} and 10^{11} g cm^{-3} (χ, the ratio of dynamic time scale to the free-fall time, is greater by 1). There is thus more time for the captures to occur, and the net result is a lower Y_l.

Since our nuclei get smaller as they heat up, the onset of the FFN restriction is at a higher density when there are no captures on protons to cool the matter. In our example, shown by the dashed line in Figures 7, 10, and 11, the entropy increased by 0.7 without proton capture (compared to a decrease of -0.2 with proton capture), which was sufficient to maintain a finite capture rate on heavies throughout the collapse. (Even though Fig. 7 shows $N \geq 40$ over a wide range of density, our method of interpolating the capture rate averages in contributions from unrestricted nuclei if N is not too much greater than 40.) The final $Y_l = 0.26$, lower than in the standard model by 0.08. Again, we see that, for the same optical depth multiplier, the trapping density when neutrinos come from heavy capture is higher than when proton-capture neutrinos dominate.

Almost half of the entropy increase is due to the excitation energy of the nucleus following capture. In model 20 we put $\Delta_n = 0$, turned off proton captures, and imposed the FFN restriction on heavy capture. The results are shown as a dotted line Figures 7, 10, and 11. The entropy increase in this model is just enough to allow a finite, but very small, capture rate. The out-of-whackness reaches 28 MeV at the trapping density $\rho_{\rm trap} = 1.5 \times 10^{12}$ g cm^{-3}, and remains high. At $\rho = 8 \times 10^{12}$ g cm^{-3}, $Z \approx 40$ and the heavy captures become allowed. The lepton fraction drops more rapidly at low density than any of the other models because the heavy-capture rate is enhanced by not having to pay the excitation energy. For the same reason this model is also less out of whack initially. The lepton fractions of this model and the corresponding standard model are equal at the trapping density of the standard model, but Y_l in model 20 decreases by only 0.01 more, even though the lower energy neutrinos from the heavy capture are trapped at a density 6 times higher.

f) *Entropy Change*

The entropy change due to neutrino processes is

$$T\dot{s} = -(\mu_\nu + \hat{\mu} - \mu_e)\dot{Y}_e - [\mu_\nu - \langle\epsilon_\nu\rangle_{\rm escape}][\dot{Y}_e + \dot{Y}_\nu] . \quad (23)$$

The first term occurs because matter is out of β-equilibrium when electrons are captured; the energy in the parentheses, the out-of-whackness, is, when positive, available for heating the matter after all Fermi levels have been paid. The second term is due to escaping neutrinos, each of which carry off, on the average, $\langle\epsilon_\nu\rangle_{\rm escape}$. These neutrinos cool the matter as long as they do not leave a hole in the neutrino distribution, i.e., as long as $\langle\epsilon_\nu\rangle_{\rm escape} \geq \mu_\nu$. Otherwise neutrinos downscatter in energy to fill the hole, and the second term represents an increase in entropy. Most of the entropy change during infall takes place before trapping, and is due to heating by the out-of-whackness and refrigeration by the escaping neutrinos. The downscatter contribution is only important on diffusive time scales which, at high densities, are much longer than the dynamical time scales we consider.

When electron captures occur on heavy nuclei only, the resulting neutrinos have, before trapping, an average energy

$$\langle\epsilon_\nu\rangle_{\rm escape} = \tfrac{3}{5}(\mu_e - \hat{\mu} - \Delta_n) = \tfrac{3}{5}(\Delta - \Delta_n) ; \quad (24)$$

and the entropy change,

$$T\dot{s} = -\dot{Y}_e[\tfrac{2}{5}\Delta + \tfrac{3}{5}\Delta_n] , \quad (25)$$

is positive. The entropy at mass $m = 0.15\ M_\odot$ is shown in Figure 12 as a function of density, for the models without electron captures on outside protons. Consider first model 20, where we also set the excitation energy to zero. Before trapping the entropy increased by $\Delta s = +0.25$, while the electron fraction changed by $\Delta Y_e = -0.10$, thus implying an average out-of-whackness $\langle\Delta/T\rangle = -(\frac{5}{2})\Delta s/\Delta Y_e = 6.25$. Most of these changes took place between the densities 10^{10} g cm^{-3}, where $\Delta/T \approx 5$, and 10^{11} g cm^{-3}, where $\Delta/T \approx 7$. These values of Δ/T are consistent with the inferred average $\langle\Delta/T\rangle$. In model 11 we again let captures occur on heavy nuclei only, but with the excitation energy given by equation (6). Figure 12 clearly shows the additional heating due to a finite Δ_n. In this model the entropy and electron fraction changed by $\Delta s = +0.74$ and $\Delta Y_e = -0.174$. If we use the average $\langle\Delta/T\rangle$ found in model 20 [Fig. 11 shows $\Delta(\rho)$ is nearly the

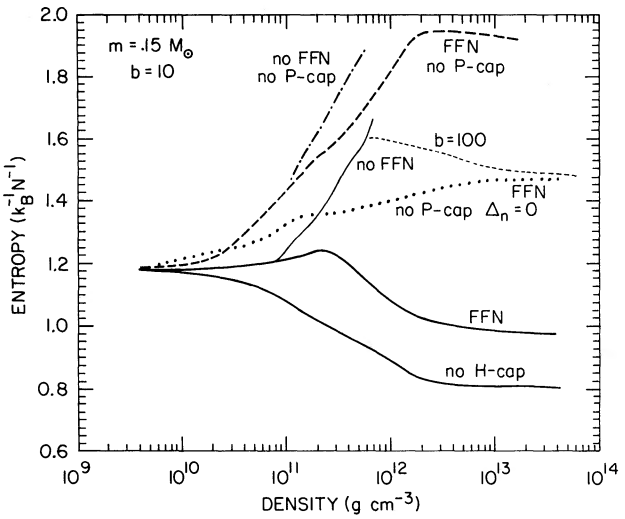

FIG. 12.—The dimensionless entropy per baryon, $s = S/k_B N$, as a function of density at mass shell $m = 0.15\ M_\odot$. The entropy increases slightly with m, but the changes in entropy with density are the same for different m. All the cases shown, with the exception noted, were computed using an optical depth multiplier $b = 10$. The label "FFN" means the FFN restriction on heavy captures was obeyed. The electron capture rate on outside protons (heavy nuclei) was set to zero for those cases labeled "no p-cap" ("no H-cap"). The excitation energy of the nucleus per electron capture Δ_n, which was set to zero for one model, is otherwise given by eq. (6).

© American Astronomical Society • Provided by the NASA Astrophysics Data System

1981ApJ...249..270V

same for these two models], we infer an average excitation energy

$$\left\langle \frac{\Delta_n}{T} \right\rangle = \left(\frac{5}{3}\right)\left[-\frac{\Delta s}{\Delta Y_e} - \frac{3}{5}\left\langle \frac{\Delta}{T} \right\rangle \right] = 2.9 . \quad (26)$$

which, since $T \approx 1$ when s and Y_e change the most, agrees very well with actual excitation energy, $\Delta_n = 3$ MeV, used in the calculation.

The neutron-proton chemical potential difference does not have to be paid in capture on outside protons, so that the resulting neutrinos, with $\langle \epsilon_\nu \rangle = \frac{5}{6}\mu_e$ (when $\mu_\nu = 0$), are more energetic than the neutrinos from capture on heavy nuclei. Because of this additional energy, and the lack of excitation of the nondegenerate free proton gas, the entropy change before trapping, $T\dot{s} = -\dot{Y}_e(\Delta - \frac{5}{6}\mu_e)$, is negative. Model 10 was calculated with captures on outside protons only. The entropy decreased by $\Delta s = -0.22$, and the electron fraction by $\Delta Y_e = -0.067$. Most of this change occurred again between the densities 10^{10} g cm^{-3}, where $(\Delta - \frac{5}{6}\mu_e)/T \approx (5 - \frac{5}{6} \times 8.4)/0.8 = -2.5$, and 10^{11} g cm^{-3}, where $(10 - \frac{5}{6} \times 16)/1.0 = -3.3$. These values of $(\Delta - \frac{5}{6}\mu_e)/T$ agree with the ratio $-\Delta s/\Delta Y_e = -3.3$.

The direction of the change of entropy with density is determined by whether electron capture is predominantly on nuclei or on outside protons. Without any restrictions on the heavy capture rates, these captures dominate captures on outside protons (except for low densities where they are comparable but where ΔY_l is small), and the entropy increases until the onset of trapping. The maximum in the entropy versus density curves, seen in Figure 13 at $\rho \approx 2 \times 10^{11}$ g cm^{-3}, is due to the onset of the FFN restriction; heavy captures dominate below this density and proton captures above. The net change of entropy during infall is, in any case, small. The entropy does increase in the complete trapping model. This model, in which the total energy of the star remains constant, is only globally adiabatic. Our adiabatic model has $\Delta s = 0$, and is both locally and globally adiabatic.

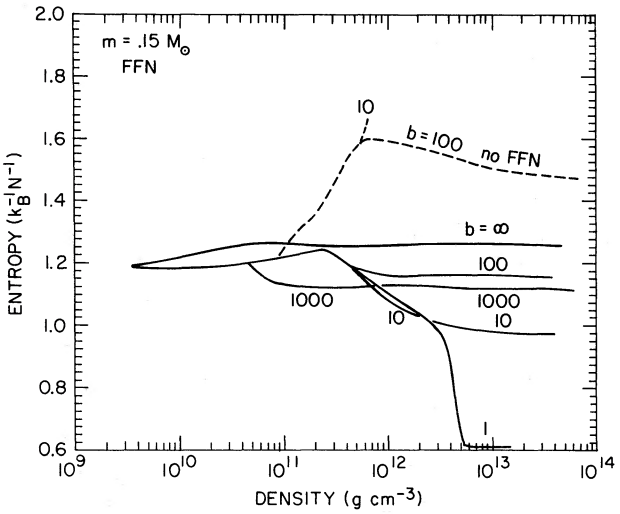

FIG. 13.—The dimensionless entropy per baryon, $s = S/k_B N$, as a function of density at mass shell $m = 0.15\ M_\odot$. The entropy increases slightly with m, but the changes in entropy with density are the same for different m. The curves are labeled with the value of the optical depth multiplier, b. The case $b = \infty$ corresponds to complete trapping of neutrinos. In all the cases, with the exception noted, electron captures on heavy nuclei obeyed the FFN restriction.

Epstein and Pethick (1981) find that the change in entropy decreases (by as much as 0.25) when they use their finite temperature capture rates rather than the $T = 0$ rates which we use. At finite temperatures electrons with energies $\epsilon_e > \mu_e$ can be captured, producing neutrinos with energies greater than we use for $\langle \epsilon_\nu \rangle$ escape in equation (23).

g) *Adiabatic Index*

The adiabatic index, $\Gamma = \partial \ln P/\partial \ln \rho$, measures how fast the pressure increases with density. If $\Gamma = (\frac{4}{3})$ [$+ O(Gm/rc^2)$ when GR is important], the increase in pressure exactly balances the increase in gravity and a homologous collapse is possible. If $\Gamma < \frac{4}{3}$, the pressure imbalance increases as the collapse proceeds, resulting in faster infall and smaller inner cores. The adiabatic index of the equation of state, $\Gamma_{\rm eos}$, evaluated at constant Y_e and s, is about $\frac{4}{3}$, as is seen in Figure 14. For low densities $\Gamma_{\rm eos} < \frac{4}{3}$ since the collapse trajectory is on the edge of the iron-alpha phase transition (where energy goes into overcoming nuclear binding energy rather than into increasing the pressure). For our adiabatic model $\Gamma_{\rm eos} < \frac{4}{3}$ over the entire collapse trajectory. The other models differ from this one by attaining a lower electron fraction at higher densities (a smaller value of b results in a smaller $Y_{e,f}$). Outside neutrons are more abundant for lower Y_e, and their $\Gamma = \frac{5}{3}$ contribution to the equation of state raises $\Gamma_{\rm eos}$ slightly above $\frac{4}{3}$. The abundance of outside neutrons also depends on the entropy, which evolves to slightly different values in the models shown, so $\Gamma_{\rm eos}$ does not increase monotonically with decreasing Y_e. Below nuclear density the combination of the strong interactions among the baryons and the Coulomb lattice energy, both of which are attractive, cause the decrease in $\Gamma_{\rm eos}$ for $\rho > 10^{13}$ g cm^{-3}.

Collapse does not take place at fixed electron fraction, nor does it take place adiabatically. (We shall nevertheless retain the usual name for Γ.) Figure 14 shows an effective adiabatic index,

$$\Gamma_H = \left.\frac{\partial \ln P}{\partial \ln \rho}\right|_{\rm collapse} , \quad (27)$$

where collapse means Γ_H was calculated along the actual trajectory of the collapse models. This index is the correct one to compare with homology criteria. If we assume the pressure is due solely to relativistic, degenerate electrons, so that $P \propto (Y_e \rho)^{4/3}$, and also assume that the electron capture neutrinos escape freely, we have for the adiabatic index

$$\Gamma_H = \frac{4}{3}\left[1 + \frac{1}{Y_e}\frac{\partial Y_e}{\partial \ln \rho}\right], \quad (28)$$

© American Astronomical Society • Provided by the NASA Astrophysics Data System

1981ApJ...249..270V

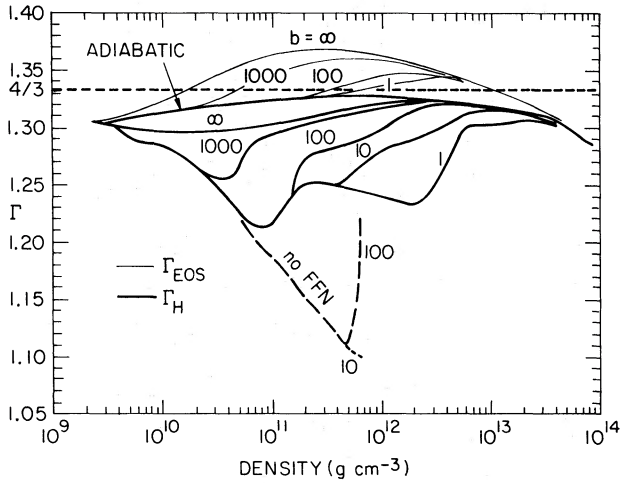

FIG. 14.—The equation of state adiabatic index, Γ_{eos} (*light curves*), and the effective adiabatic index, Γ_H (*heavy curves*), as a function of density at mass shell $m = 0.15\ M_\odot$, for several collapse models. The equation of state index is calculated at constant electron fraction and entropy. The effective index reflects the pressure actually found in the calculations, and is lower than the equation of state index due to neutrino emission and neutronization. The curves are labelled by the value of the optical depth multiplier, b. The case $b = \infty$ corresponds to complete trapping where neutrinos, once created, never escape. The two indices are equal for the adiabatic model, where the electron fraction remains constant. In all models, with the exception noted (*dashed line*), the electron capture rates on heavy nuclei were restricted according to the FFN criterion.

which agrees with the model results below the trapping density. As is verified by comparing Figures 14 and 8, more rapid electron loss leads to a lower effective adiabatic index (and hence more rapid collapse). The decrease in the capture rate due to the onset of the FFN restriction at $\rho \approx 10^{11}$ g cm^{-3} is clearly reflected in the increase in Γ_H above that density.

After trapping, neutrinos also contribute to the pressure. Assuming then that only the electrons and neutrinos contribute and also that $\partial Y_\nu/\partial\rho = -\partial Y_e/\partial\rho$, the adiabatic index would be

$$\Gamma_H = \frac{4}{3}\left[1 + \frac{(Y_e^{1/3} - \frac{1}{2}^{1/3} Y_\nu^{1/3})\partial Y_e/\partial \ln \rho}{Y_e^{4/3} + \frac{1}{2}^{1/3} Y_\nu^{4/3}}\right], \quad (29)$$

where the factor of $\frac{1}{2}$ reflects the lower statistical weight of the neutrinos. The effective adiabatic index increases, as a function of density, once the trapping density is exceeded, usually attaining its minimum value at the trapping density. Just above the trapping density, the neutrino fraction Y_ν, although unimportant in the above formula, leads, through the blocking of final states in the capture reaction, to a reduced decrease of the electron fraction. As the density increases further, the electron fraction and entropy change less rapidly with density, the neutrino fraction increases, and the baryon contribution to the equation of state becomes more important; all these effects lessen the difference between the effective adiabatic index and the equation of state index at higher densities.

h) *Homologous Collapse?*

If the adiabatic index $\Gamma = \frac{4}{3}$ exactly, if the pressure deficit, $d = P/P_0(\rho/\rho_0)^{4/3}$, relative to a $\gamma = \frac{4}{3}$ trajectory, is constant, and if GR effects are negligible, the evolution of an inner fraction of the core is exactly homologous. (We distinguish between homologous, where $U \propto r$ at each instant, and exactly homologous, where the mass of the homologous core remains constant throughout the collapse.) Our realistic collapses violate all three criteria, and do not show an exactly homologous collapse (see Fig. 4*a*). At each instant, however, the inner core is roughly homologous, and some homology results apply. We compare our models with the results of Goldreich and Weber (1980; hereafter GW) who give analytic solutions for the idealized case.

Exactly homologous motion means that the mass and time dependence of the density evolution are separable, i.e., $\rho(m, t) = \rho_0(m)f(t)$. The subscript zero will always stand for the initial model. Since the density profile remains similar, the density scales with radius as $\rho(m) \propto r(m)^{-3}$. By taking time derivatives of the above two equations, we have

$$\rho_0(m)\dot{f}(t) = \dot{\rho} = -3\rho\dot{r}(m)/r(m) = \rho_0(m)f(t)U(m)/r(m)\,, \quad (30)$$

where $U = \dot{r}$ is the velocity. We see that U/r is independent of m; we set $U(m, t) = v(t)r(m)$. Our density profiles do not remain similar (Fig. 4*a*)—the mass of the inner core decreases as the collapse proceeds.

It is customary to measure the rate of collapse by the ratio, χ, of the dynamical time scale to the free-fall time scale,

$$\chi = [\rho/\dot{\rho}]/[(24\pi G\rho)^{-1/2}]\,. \quad (31)$$

For homologous collapse,

$$\chi = (24\pi G)^{1/2}\rho_0^{1/2}(m)f(t)^{3/2}/\dot{f}(t)$$
$$= (24\pi G)^{1/2}\rho_0^{1/2}(m)f(t)^{1/2}/[3v(t)]\,. \quad (32)$$

Thus the outer layers of the homologous core collapse more quickly, relative to the local free-fall rate, than the center. In our initial model $\rho_0(0) = 5.8 \times 10^9$ g cm^{-3}, while $\rho_0(0.5\ M_\odot) = 1.7 \times 10^9$ g cm^{-3}, so $\chi(0) = 1.85\ \chi(0.5\ M_\odot)$. Collapse will proceed no faster than free-fall ($\chi = 1$). The mass of the homologous inner core satisfies $\chi(M_{IC}) \approx 1$. The outer core ($m > M_{IC}$) is left behind in free fall. In the exactly homologous solution of GW, χ, at the center of the core, remains constant in time and is given by $\chi = \lambda^{-1/2}$, where λ is GW's separation constant. In our models χ decreases rapidly with density (Fig. 15).

Since the capture rates and neutrino mean free path depend strongly on density, but not much on mass, we consider collapse rate for different shells, m_1 and m_2, as they pass through the same density, ρ_*. The times t_1 and t_2 are taken to satisfy $\rho(m_1, t_1) = \rho_* = \rho(m_2, t_2)$. If exact homology is assumed, it can be shown that the collapse

© American Astronomical Society • Provided by the NASA Astrophysics Data System

1981ApJ...249..270V

rates are again related by the root of the initial densities for these shells:

$$\frac{\chi(m_1, \rho_*)}{\chi(m_2, \rho_*)} = \left[\frac{f(t_2)}{f(t_1)}\right]^{1/2} = \left[\frac{\rho_0(m_1)}{\rho_0(m_2)}\right]^{1/2}. \quad (33)$$

In Figure 15 we show $\chi(\rho)$ for $m = 0.15$, 0.30, and 0.50 $M_\odot$. These shells have initial densities of 4.0, 2.8, and 1.7×10^9 g cm^{-3}, respectively. By equation (33) we would expect

$$\chi(0.15\ M_\odot)/\chi(0.5\ M_\odot) = 1.5.$$

The spacing found in the figure is slightly larger than this, increasing from a factor 2 at low density to 2.5 for $\rho > 10^{11}$ g cm^{-3}. Since χ is decreasing with density (and time), $f(t_2)/f(t_1)$ is larger than if χ were constant in time, resulting in the larger spacing we see in Figure 15. In the initial model χ is large ($\gtrsim 20$), but decreases rapidly with increasing density. When the density $\rho = 10^{11}$ g cm^{-3}, $\chi = 7$ at $m = 0.15\ M_\odot$, and $\chi = 3$ further out at $m = 0.5\ M_\odot$. When the central density reaches 10^{14} g cm^{-3}, χ has decreased to about one-half of these values.

Figure 15 shows the results of model 9. The $\chi(\rho)$ curves for the other nonadiabatic models are similar, with larger lepton losses resulting in slightly faster collapse (smaller χ). When mass shell $m = 0.15$ attained a density of 4×10^{13} g cm^{-3}, the complete trapping model ($b = \infty$) was collapsing with $\chi = 4.5$, while model 8 ($b = 1$), with a final $Y = 0.31$, had $\chi = 3.2$. The adiabatic model collapsed more slowly than the others. In Table 1 we give $\chi(m = 0.15\ M_\odot)$ and $\chi(m = 0.5\ M_\odot)$ when $\rho_c = 10^{14}$ g cm^{-3}.

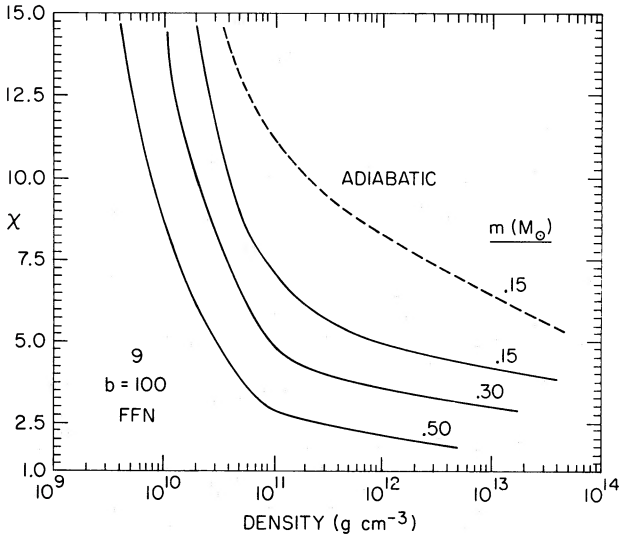

FIG. 15.—The ratio, χ, of the dynamical time scale to the free-fall time scale, as a function of density for mass shells $m = 0.15$, 0.3, and 0.5 $M_\odot$. Free-fall corresponds to $\chi = 1$. The case shown in model 9, for which the optical depth multiplier $b = 100$ and electron captures on heavy nuclei were restricted by the FFN criterion. The results for the other nonadiabatic models are similar, with a lower lepton fraction resulting in a slightly smaller χ. The dashed line is for the mass shell $m = 0.15\ M_\odot$ of the adiabatic model.

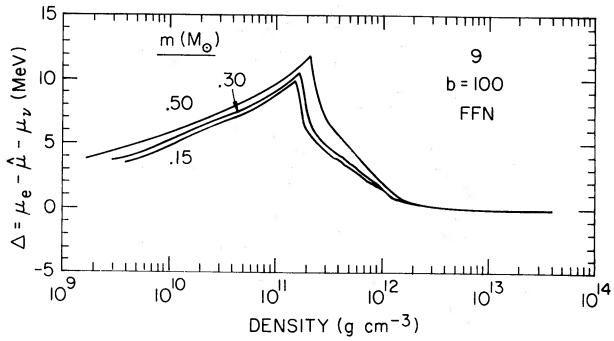

FIG. 16.—The "out-of-whackness," $\Delta = \mu_e + \mu_p - \mu_n - \mu_\nu = \mu_e - \hat{\mu} - \mu_\nu$, as a function of density for mass shells $m = 0.15$, 0.3, and 0.5 $M_\odot$. The case shown is model 9, for which the optical depth multiplier $b = 100$ and electron captures on heavy nuclei were restricted by the FFN criterion.

Figure 16 shows the out-of-whackness for the same mass shells shown in Figure 15. Even though the outer shell ($m = 0.5\ M_\odot$) is collapsing twice as fast as the inner shell ($m = 0.15\ M_\odot$), it is only 1 MeV more out-of-whack (at the same density) before trapping. Figure 16 also shows that the trapping density is higher in the outer shell ($\rho_{\rm trap} = 2.3 \times 10^{11}$ g cm^{-3}) than in the inner one ($\rho_{\rm trap} = 1.6 \times 10^{11}$ g cm^{-3}). The density gradient above the outer shell is steeper than the gradient above the inner shell when $\rho = 10^{11}$ g cm^{-3} for these shells (see Fig. 4*a*). Because of the steeper gradient the optical depth is less, so the outer shell must evolve to a higher density before the optical depth required for trapping is attained.

i) Pressure Deficit

The pressure deficit, as a function of density, is shown for several mass shells in Figure 17. The decrease with density (showing again that the collapse is not exactly homologous) is just a reflection of the unstable effective adiabatic index (i.e., $\Gamma_H < \frac{4}{3}$). If the pressure is dominated by electrons and neutrinos, the pressure deficit would be

$$d_Y = \frac{(Y_{e,f})^{4/3} + \frac{1}{2}^{1/3}(Y_{\nu,f})^{4/3}}{(Y_{e,0})^{4/3}}, \quad (34)$$

where the subscripts 0 and f stand for the initial and final values, respectively. This quantity[7] is tabulated in Table 1, along with the pressure deficit, d, actually found in the collapse calculations. The latter is about 15% and 20% lower than d_y (except for $Y_{l,f} < 0.26$). This discrepancy is due to the departure from $\frac{4}{3}$ of the baryon contribution to the adiabatic index. If we assume $\hat{\mu} = 0$, so that $Y_{e,f} = \frac{2}{3}Y_{l,f}$ is less than the realistic value, equation (34) gives a pressure deficit which is smaller than the actual value (except for the largest $Y_{l,f} = 0.43$).

[7] The values of d_y given in Table 1 were incorrectly calculated with the neutrino contribution multiplied by $\frac{1}{2}$, rather than $\frac{1}{2}^{1/3}$, and are thus a few percent too small.

© American Astronomical Society • Provided by the NASA Astrophysics Data System

1981ApJ...249..270V

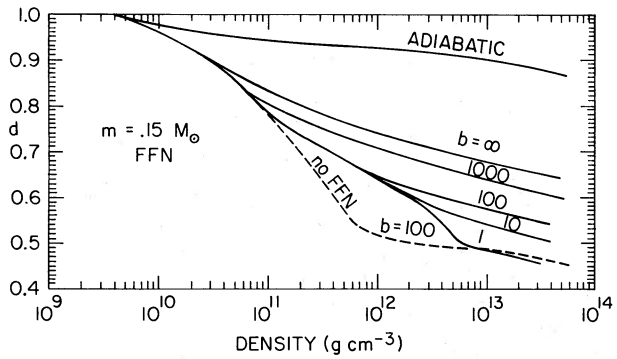

FIG. 17.—The pressure deficit, d, as a function of density at mass shell $m = 0.15\ M_\odot$, for several collapse models. The curves are labeled by the value of the optical depth multiplier, b. The case $b = \infty$ corresponds to complete trapping where neutrinos, once created, never escape. The electron fraction remained constant in the adiabatic model. In all models, with the exception noted (*dashed line*), the electron capture rates on heavy nuclei were restricted according to the FFN criterion. An overlying mass shell has a smaller initial density, and therefore has a slightly lower pressure deficit at a given density.

j) *Instantaneous Homology*

Exactly homology does not hold for these realistic collapses, but at each instant in the collapse there is an inner core for which the velocity is (roughly) proportional to the radius. The mass of this inner core can usually be predicted from the solution of GW, who find

$$M_{\rm GW} = 1.0449 d^{3/2} M\ , \tag{35}$$

where M is the mass of the initial equilibrium $n = 3$ polytrope. The equation of state assumed by GW is $P = K\rho^{4/3} = dK_0\,\rho^{4/3}$, where K_0 is the pressure constant in equilibrium. An iron core supported by relativistic electron pressure is well approximated by such polytropic distribution. Our initial model, however, is not in equilibrium. Instead, we identify M with the homologously collapsing mass in the initial model, the boundary of which we take to be the maximum in the infall velocity. Since the velocity profile is rather shallow between 1.4 and 1.6 $M_\odot$, we take $M = 1.57\ M_\odot$ so that the inner core mass $[m(U_{\rm min})]$ of the non-GR adiabatic model agrees with the Goldreich and Weber result.

In Table 1 we compare the Goldreich and Weber homologous mass with the mass of our inner cores, when the central density has just reached $\rho_c = 10^{14}$ g cm^{-3}. At this central density the effective adiabatic index is close to $\frac{4}{3}$ ($\Gamma_H \approx 1.30$) throughout most of the inner core, so that we might expect the $\Gamma = \frac{4}{3}$ solution to be approximately valid. The corrections due to GR are about 5% at this density. We use the actual pressure deficit at $m = 0.15\ M_\odot$ at that instant in computing $M_{\rm GW}$. We give two values for our mass. The first is the mass at the minimum of the velocity $m(U_{\rm min})$, interior to which $U \propto r$. We also list the mass at the sonic point, $m_{\rm sonic}$, where the matter and sound velocities are equal in magnitude. Sound waves originating at the center cannot propagate past this point on a dynamical time scale. The sonic point is always interior to the minimum in velocity.

The Goldreich and Weber mass we calculate is usually between the sonic mass and the minimum velocity mass, being in most cases closer to the latter. For all collapse models $m_{\rm GW} > m_{\rm sonic}$. The exceptions to $m_{\rm GW} < m(U_{\rm min})$ are (1) models 8 and 30, which have the smallest inner cores and the largest pressure deficits, and (2) the GR adiabatic model (14) for which GR effects are strongest, since the effective adiabatic index is close to $\frac{4}{3}$ throughout the collapse.

V. GENERAL RELATIVISTIC CORRECTIONS

a) *Initial Model*

The initial model for our GR hydrodynamics has been evolved under Newtonian gravity. Since the adiabatic index of the core is close to the critical value $\frac{4}{3}$, GR corrections are important if the core is not very much out of equilibrium. The equation of motion in GR is

$$e^{-\phi}\frac{\partial U}{\partial t} = -\frac{4\pi[1 + (U/c)^2 - 2G\tilde{m}/c^2 r]^{1/2} r^2}{1 + E/c^2 + PV/c^2}\frac{\partial P}{\partial m} - \frac{G}{r^2}\left(\tilde{m} + \frac{4\pi r^3 P}{c^2}\right), \tag{36}$$

where e^ϕ is the redshift, and the gravitational mass $\tilde{m}$ differs from the rest mass m by

$$\tilde{m}(m) = \int_0^m \left(1 + \frac{E}{c^2}\right)\left[1 + \left(\frac{U}{c}\right)^2 - \frac{2G\tilde{m}}{rc^2}\right]^{1/2} dm\ . \tag{37}$$

The largest GR "correction" is the internal energy term, E/c^2, which is dominated by the binding energy of the iron peak nuclei. For a binding energy $E = -8.6$ MeV per nucleon, $E/c^2 - 0.009$. The next largest correction is the ratio of the Schwarzschild and stellar radii. $2Gm/rc^2$, which has a maximum value of 0.004 (at $m = 1\ M_\odot$), but enters only in a square root. The two terms involving the pressure, $4\pi r^3 P/mc^2$ and PV/c^2, have maximum values of 0.0024 and 0.0009, respectively, at the center. The special relativity correction, $(U/c)^2$, is at most 7×10^{-6}. In addition to being smaller in magnitude than the internal energy correction, which is constant throughout the core, these other terms are smaller away from where they peak. Since the negative energy correction increases the pressure gradient and reduces the gravitational mass, it will reduce the acceleration and, if the core is sufficiently close to equilibrium, lead to expansion. The importance of this term can be diminished by merely redefining the zero of energy. We shifted our internal energy scale by adding 8.64 MeV per baryon, thus canceling the effects of the large binding energy. The magnitude of the resultant energy correction is comparable to the size of PV/c^2, and our gravitational mass and pressure gradient differ by no more than two-tenths of a percent from the Newtonian model.

The remaining corrections are important only if they are comparable to the pressure imbalance, i.e., the ratio of the two terms in the acceleration equation. (We could not compute the initial imbalance directly because of numerical jitter.) Whatever the initial imbalance, it will increase with increasing density since the adiabatic index at the

© American Astronomical Society • Provided by the NASA Astrophysics Data System

1981ApJ...249..270V

center of the core $\Gamma = 1.305$ is less than $\frac{4}{3}$. If collapse continues as fast as in the initial model for a sound crossing time of the homologous core, the pressure imbalance will increase by a percent, thus becoming larger than the remaining GR corrections.

b) *Infall*

Several collapse models were computed using Newtonian hydrodynamics. The Newtonian models took about 15% longer than the corresponding GR model to reach a central density $\rho_c = 10^{14}$ g cm^{-3}. Nearly all of this additional time was spent at densities within a factor of 2 of those in the initial model, where GR terms were still comparable to the pressure imbalance.

Figure 18 shows the collapse rate for the adiabatic model and for a more realistic model evolved under both GR and Newtonian hydrodynamics. The effects of GR are largest in the adiabatic model. In that model, the adiabatic index $\Gamma_H = \Gamma_{\rm eos} \lesssim \frac{4}{3}$. The important quantity for the hydrodynamics is $\Gamma_{\rm cr} - \Gamma_H$, where $\Gamma_{\rm cr} = \frac{4}{3} + O(Gm/rc^2)$ is the adiabatic index for which neutral stability obtains. When the difference $\Gamma_H - \frac{4}{3}$ is comparable to the GR corrections, GR has a large effect on the evolution. The realistic model, on the other hand, has an effective adiabatic index $\Gamma_H \ll \frac{4}{3}$, and we see little difference in the collapse rate until the highest densities, where GR terms become large and the effective adiabatic index approaches $\frac{4}{3}$.

Because of the nearly equal collapse rates the lepton fractions, entropy, out-of-whackness, pressure deficit, etc., have the same density dependence in the Newtonian models as in the GR models. The inner core mass in the Newtonian models is 10% larger when measured at the velocity minimum (20% if measured at the sonic point). The larger inner core mass leads to a slightly higher maximum infall velocity in the Newtonian models (-3.7×10^9 cm s^{-1} compared with -3.5×10^9 cm s^{-1} for models with $b = 100$).

Although GR effects are not big in the collapse up to $\rho_c = 10^{14}$ g cm^{-3}, they should not be neglected for the subsequent evolution (especially if a black hole results). Under GR a higher density is reached at bounce, and the postbounce oscillations are damped much more rapidly than in the Newtonian limit.

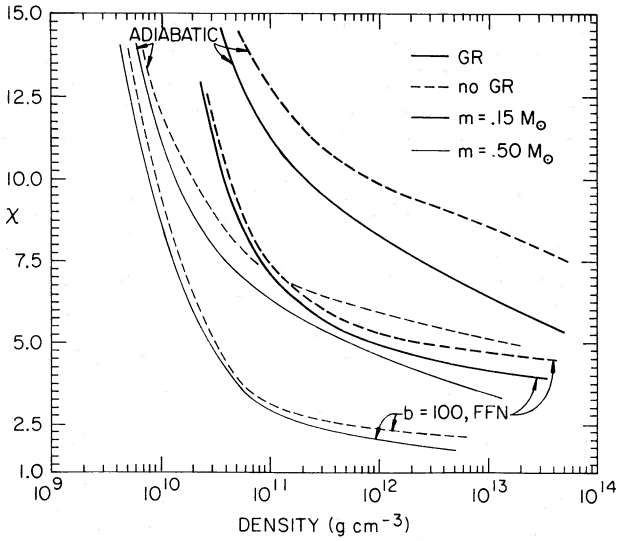

FIG. 18.—The ratio of the dynamical time scale to the free-fall time scale, χ, for models calculated with GR hydrodynamics (*solid lines*) and Newtonian hydrodynamics (*dashed lines*), as a function of density for mass shells $m = 0.15\ M_\odot$ (*dark lines*) and $m = 0.5\ M_\odot$ (*light lines*). The two cases shown are (1) the adiabatic model where the GR effects are large because the effective adiabatic index is close to $\frac{4}{3}$, and (2) a more realistic model (9), with an optical depth multiplier $b = 100$ and the FFN restriction on electron capture by nuclei, for which GR effects are slight until high density.

VI. CONCLUSIONS

During the collapse of a 1.5 $M_\odot$ stellar core most of the baryons reside in nuclei. For our realistic models, in which the entropy does not change much during infall ($1.1 \leq s \leq 1.6$), the mass fraction of heavy nuclei $X_H \approx 0.9$. Alpha-particles contribute $X_\alpha \approx 0.1$ below 10^{11} g cm^{-3}, and outside neutrons have $X_n \approx 0.1$ above that density. The outside proton fraction remains between 10^{-3} and 10^{-4}.

The neutron number N of the typical heavy nucleus exceeds 40 for $\rho > \rho_{40} \approx 10^{11}$ g cm^{-3}. The suppression of the electron capture rate on heavy nuclei for $N \geq 40$ (FFN) strongly affects the lepton fraction at bounce ($Y_{l,f} = 0.36$ with this FFN suppression, $= 0.27$ without) and consequently the mass of the inner homologous core at bounce ($M_{\rm IC} = 0.71\ M_\odot$ with, $= 0.49\ M_\odot$ without).

For densities less than about 10^{11} g cm^{-3} the rates of electron capture on outside protons and heavy nuclei are comparable. For higher densities the rate on nuclei, if not suppressed, dominates. The cooling of the matter by captures on outside protons is important in determining ρ_{40}. We find that when capture proceeds solely on heavy nuclei, the increase in entropy and the consequent decrease in nuclear size keep $N \leq 40$ throughout the infall, so that rapid electron capture on nuclei persists until neutrino trapping.

Because the nuclear shell model predicts a strong dependence of capture rates on N and Z, the outcome of collapse is sensitive to (1) the abundances of outside protons, (2) the size of the heavy nucleus for densities between 10^{10} and 10^{12} g cm^{-3}, electron fractions between 0.45 and 0.25, and entropies between 1 and 2, and (3) the spread of an ensemble of nuclei about the typical heavy values. The LLPR equation of state may be used to estimate X_p and the heavy properties accurately; we will report elsewhere on distribution of N found in a nuclear statistical equilibrium model.

The rate of collapse, as measured by the ratio of the dynamical time scale to the free-fall time scale, χ, decreases rapidly with increasing density, from about $\chi = 7$ at 10^{11} g cm^{-3} to $\chi \lesssim 4$ at 10^{14} g cm^{-3}. Farther out in the core the ratio is even smaller than these central values. The evolution, with density, of the entropy, lepton fractions, and the out-of-whackness are rather insensitive to changes in χ.

© American Astronomical Society • Provided by the NASA Astrophysics Data System

1981ApJ...249..270V

The evolution, with density, of each mass element is similar, resulting in a flat lepton distribution for densities greater than the neutrino trapping density.

During infall the pressure is dominated by electrons and neutrinos. The adiabatic index of the matter at constant Y_e is close to $\frac{4}{3}$. The departure of the effective adiabatic index from $\frac{4}{3}$ is due mostly to the changes of the electron and neutrino fractions with density. The pressure deficit calculated from the initial and final lepton fractions underestimates the actual deficit by about 20%.

The infall is not exactly homologous—during infall the density distribution becomes more centrally peaked, the rate of collapse, χ, decreases, and the pressure imbalance increases.

At each instant, however, there is a homologous inner core where the velocity is proportional to the radius. The mass of this inner core agrees with the formula of Goldreich and Weber, equation (35), to 20%.

General-relativistic effects are small during the infall. The inner core mass is about 10% less in a GR model, as compared to a Newtonian model. The evolution of the lepton fractions, entropy, etc., are nearly the same in corresponding GR and Newtonian models.

This work has benefited from the advice of a number of people, among them S. A. Colgate, M. J. Newman, G. Fuller, C. J. Pethick, S. W. Hodson, S. E. Woosley, J. R. Wilson, W. A. Fowler, W. D. Arnett, and D. G. Ravenhall. We are grateful for the hospitality of the Aspen Center for Physics, the Institute of Theoretical Physics at Santa Barbara, and especially Los Alamos Scientific Laboratory, where the models were calculated.

REFERENCES

Arnett, W. D. 1967, *Canadian J. Phys.*, **45**, 1621.
———. 1977*a*, *Ap. J. Suppl.*, **35**, 145.
———. 1977*b*, *Ap. J.*, **218**, 815.
———. 1978, *Ap. J.*, **219**, 1008.
Arnett, W. D., and Falk, S. W. 1976, *Ap. J.*, **210**, 733.
Baade, W., and Zwicky, F. 1934, *Proc. Nat. Acad. Sci.*, **20**, 259.
Barkat, Z. 1977, in *Supernovae*, ed. D. N. Schramm (Dordrecht: Reidel), p. 131.
Bethe, H. A., Applegate, J., and Brown, G. E. 1980, *Ap. J.*, **241**, 343.
Bethe, H. A., Brown, G. E., Applegate, J., and Lattimer, J. M. 1979, *Nucl. Phys. A*, **324**, 487 (BBAL).
Bludman, S. A., and Van Riper, K. A. 1978, *Ap. J.*, **224**, 631.
Bond, J. R. 1978, Ph.D. thesis, California Institute of Technology.
Bruenn, S. W. 1975, *Ann. NY Acad. Sci.*, **262**, 80.
Canizares, C. R., and Winkler, P. F. 1981, *Ap. J. (Letters)*, **246**, L33.
Chevalier, R. A. 1976, *Ap. J.*, **207**, 872.
Chevalier, R. A., and Kirshner, R. P. 1978, *Ap. J.*, **219**, 931.
Colgate, S. A. 1978, *Mem. Soc. Astr. Italiana*, Vol. **49**, No. 2–3.
Colgate, S. A., and Petschek, A. G. 1980, *Ap. J. (Letters)*, **236**, L115.
Colgate, S. A., and White, R. H. 1966, *Ap. J.*, **143**, 626.
Epstein, R. I. 1979, *M.N.R.A.S.*, **188**, 305.
Epstein, R. I., Nørgaard, H., and Bond, J. R. 1979, *Astr. Ap.*, **74**, 353.
Epstein, R. I., and Pethick, C. J. 1981, *Ap. J.*, **243**, 1003.
Fuller, G., Fowler, W. A., and Newman, M. J. 1981, in preparation (FFN).
Fuller, G. 1980, private communication.
Goldreich, P., and Weber, S. V. 1980, *Ap. J.*, **238**, 991 (GW).
Grasberg, E. K., Imshennik, V. S., and Nadyozhin, D. K. 1971, *Ap. Space Sci.*, **10**, 28.
Lamb, D. Q., Lattimer, J. M., Pethick, C. J., and Ravenhall, D. G. 1978, *Phys. Rev. Letters*, **41**, 1623 (LLPR).
———. 1981, in preparation (LLPR).
Lamb, S. A. 1978, *Ap. J.*, **220**, 186.
Lasher, G. 1975, *Ap. J.*, **210**, 194.
Lattimer, J. M., and Ravenhall, D. G. 1978, *Ap. J.*, **223**, 314.
Lattimer, J. M., and Mazurek, T. J. 1981, *Ap. J.*, **246**, 955.
Lichtenstadt, I., Sack, N., and Bludman, S. A. 1980, *Ap. J.*, **237**, 903.
May, M., and White, R. H. 1967, *Meth. Comput. Phys.*, **7**, 219.
Sato, K. 1975, *Progr. Theor. Phys.*, **54**, 1325.
Schramm, D. N., and Arnett, W. D. 1975, *Phys. Rev. Letters*, **34**, 113.
Schwartz, R. A. 1967, *Ann. Phys.*, **43**, 42.
Tubbs, D. L., and Schramm, D. N. 1975, *Ap. J.*, **201**, 467.
Van Riper, K. A. 1978, *Ap. J.*, **221**, 304.
———. 1979, *Ap. J.*, **232**, 558.
———. 1980, *Ap. J.*, **240**, 658.
Weaver, T. A., and Woosley, S. E. 1980, *Ann. NY Acad. Sci.*, **336**, 335.
Weaver, T. A., Zimmerman, G. B., and Woosley, S. E. 1978, *Ap. J.*, **225**, 1021 (WZW).
Wilson, J. R. 1971, *Ap. J.*, **163**, 209.
———. 1980*a*, *Ann. NY Acad. Sci.*, **336**, 358.
———. 1980*b*, private communication.

Note added in proof.—The chemical potential difference Δ_H (eq. [2]) or, in the presence of a neutrino sea, $\Delta - \Delta_n$ (eq. [3]) is the maximum energy of a neutrino produced by electron capture on a heavy nucleus. The inhibition of the capture rates by neutrino degeneracy was incorporated in the rates (eqs. [5] and [9]) by replacing the lower limit on the integral in equation (1) with μ_ν. This procedure assumes the neutrinos are completely degenerate. The value of Γ_H given in Table 1 was calculated by equation (27), not by the approximate equations (28) and (29). The relation between the collapse rate χ and Goldreich and Weber's constant λ, $\chi = \lambda^{-1/2}$, is valid only when $r(m) \ll r_0(m)$, i.e., only when the density has increased several orders of magnitude from the initial model.

JAMES M. LATTIMER: Department of Earth and Space Sciences, State University of New York at Stony Brook, Stony Brook, NY 11794

KENNETH A. VAN RIPER: MS 625 X-7, Los Alamos National Laboratory, P.O. Box 1663, Los Alamos, NM 87545

© American Astronomical Society • Provided by the NASA Astrophysics Data System